2012

Characterization, Morphology, Oxidation, And Recession Of Silicon Nanowires Grown By Electroless Process

Robert G. Mertens
University of Central Florida

CHARACTERIZATION, MORPHOLOGY, OXIDATION AND RECESSION OF SILICON NANOWIRES GROWN BY ELECTROLESS PROCESS

by

ROBERT GEORGE MERTENS
B.S.E.T. University of Central Florida
B.S. Phys. University of Central Florida
M.S.E.E. University of Central Florida

A dissertation submitted in partial fulfillment of the requirements
for the degree of Doctor of Philosophy
in the Department of Electrical Engineering and Computer Science
in the College of Engineering and Computer Science
at the University of Central Florida
Orlando, Florida

Summer Term
2012

Major Professor: Kalpathy B. Sundaram

ABSTRACT

This dissertation presents heretofore undiscovered properties of Silicon Nanowires (SiNWs) grown by electroless process and presents mathematical solutions to the special problems of the oxidation and diffusion of dopants for SiNWs. Also presented here is a mathematical description of morphology of oxidized SiNWs. This dissertation is comprised of several discussions relating to SiNWs growth, oxidation, morphology and doping.

In here is presented work derived from a long-term study of SiNWs. Several important aspects of SiNWs were investigated and the results published in journals and conference papers. The recession of SiNWs was heretofore unreported by other research groups. In our investigations, this began as a question, "How far into the substrate does the etching process go when this method is used to make SiNWs?" Our investigations showed that recession did take place, was controllable and that a number of variables were responsible. The growth mechanism of SiNWs grown by electroless process is discussed at length. The relation of exposed area to volume of solution is shown, derived from experimentation. A relation of Silver used to Si removed is presented, derived from experimentation. The agglomeration of SiNWs grown by the electroless process is presented.

The oxidation of SiNWs is a subject of interest to many groups, although most other groups work with SiNWs grown by the VLS process, which is more difficult, time-consuming and expensive to do. The oxidation of planar Silicon (Si) is still a subject of study, even today, after many years of working with and refining our formulae, because of the changing needs of this science and industry. SiNWs oxidation formulae are more complicated than those for planar Si, partly because of their morphology and partly because of their scale. While planar Si only

presents one orientation for oxidation, SiNWs present a range of orientations, usually everything between <100> and <110> (the <111> orientation is usually not presented during oxidation). This complicates the post-oxidation morphology to the extent that, subsequent to oxidation, SiNWs are more rectangular than cylindrical in shape. After etching to remove an oxidation layer from the SiNWs, the rectangular shape shifts 90° in orientation.

In traditional oxidation, the Deal-Grove formulae are used, but when the oxidation must take place in very small layers, such as with nanoscale devices, the Massoud formulae have to be used. However, even with Massoud, these formulae are not as good because of the morphology. Deal-Grove and Massoud formulae are intended for use with planar Si. We present some formulae that show the change in shape of SiNWs during oxidation, due to their morphology.

The diffusion of dopants in SiNWs is a subject few research groups have taken up. Most of the groups who have, use SiNWs grown by the VLS method to make measurements and report findings. In order to measure the diffusion of dopants in SiNWs, a controllable diameter is needed. There are a number of ways to measure diffusion in SiNWs, but none of the ones used so far apply well to SiNWs grown by electroless process. Usually these groups present some mathematical formulae to predict diffusion in SiNWs, but these seem to lack mathematical rigor. Diffusion is a process that is best understood using Fick's Laws, which are applied to the problem of SiNWs in this dissertation.

Diffusion is a science with a long history, going back at least 150 years. There are many formulae that can be used in the most common diffusion processes, but the processes involved with the diffusion of dopants in SiNWs is more complex than the simple diffusion processes that are fairly well-understood. Diffusion doping of SiNWs is a multiphase process that is more complex, first because it is multiphase and second because the second step involves a

multiplicity of diffusing elements, plus oxidation, which brings on the problems of moving boundaries.

In this dissertation, we present solutions to these problems, and the two-step diffusion process for SiNWs.

To each person in my life who helped make it happen.

To each person who inspired me.

To each person who cared.

ACKNOWLEDGMENTS

Special thanks to my advisor, my teacher, and especially, my friend, Dr. Kalpathy B. Sundaram, who, above all other things, believed in me.

Special thanks to my sister, Joyce E. Mertens, who helped me finance this great escapade, because she believes in escapades, so long as they are not her own.

To my good friend and co-adviser, Dr. Louis C. Chow, who also helped me finance this operation, but may not necessarily believe in escapades.

Special thanks to the members of my Doctoral Committee, for their participation, Dr. Jiann S. Yuan, Dr. Parveen Wahid, and Dr. Richard Blair.

Thanks to Wei Wu for his help with the equations.

There are many other people who contributed to my graduate school pursuits, and that list could go on for days. My thanks go out to all of you.

TABLE OF CONTENTS

LIST OF FIGURES

LIST OF TABLES

LIST OF ACRONYMS/ABBREVIATIONS

Å - Angstroms

α_n's are the positive roots of $J_0(R\alpha_n) = 0$

nn° - angular degrees (where nn is a number)

°C – Degrees centigrade/Celsius

π – pi, the number 3.14159…

ρ - Resistivity

τ - time for the pre-existing oxidation layer

τ_1, τ_2 - constants defined by experimental results

θ – angle in radians

Ω-cm – Ohm-centimeter

μm – microns

A_F - area amplification factor

Ag - Silver

Ag^+ - Silver positive ion

Ag_2O – Silver oxide

$AgNO_3$ – Silver nitrate

AgOH – Silver hydroxide

AM1.5 - air mass 1.5

A_{NW} - Area of a single SiNW

(aq) - Aqueous

AR - Antireflective

A_T - Total area

A_W - Area of the wafer

B - linear rate constant

B/A - parabolic rate constant

BOE – Buffered oxide etch

C_0 – surface doping concentration during pre-dep

cm – centimeters

cm^2 – square centimeters

CVD - Chemical vapor deposition

d - average diameter of the SiNWs

D - distance between SiNWs centers

D – diffusivity

D_0 - diffusion coefficient

DI H_2O – Deionized water

d_{NW} - average diameter of SiNWs

e^- - Negative electron charge

E_A – activation energy

EDS - Energy-dispersive X-ray spectroscopy

E-beam – Electron beam

eV – Electron volts

H_2O_2 – Hydrogen peroxide

HF – Hydrofluoric acid

HNO_3 - Nitric acid

H_{NW} - average height of the SiNWs

k_B – Boltzman constant

M – Molar, molarity, moles

M_0, M_1 and M_2 - constants defined by experimental results

mg – milligrams

min. - minutes

ml - milliliters

mm^2 – square millimeters

N_2 – Nitrogen (gaseous)

N_{B0} – surface concentration for Boron during pre-dep

nm - nanometers

n_{NW} - average number is SiNWs per unit area

N_{NW} - total number of SiNWs on the wafer

N_{P0} - surface concentration for Phosphorus during pre-dep

NWs - Nanowires

PECVD - plasma-enhanced CVD

PR - photoresist

r_0 – radius of the pre-oxidized SiNW (radius of the original unoxidized SiNW)

r_1 – outside radius of the oxidized SiNW

r_2 –radius of the unoxidized SiNW beneath the oxidation layer

$r_1'(\theta)$ – ratio of expansion contribution of SiO_2 in the (100) plane during oxidation

$r_2''(\theta)$ - ratio of expansion contribution of SiO_2 in the (110) plane during oxidation

R - initial radius of the SiNWs

(s) - solid

SEM - scanning electron microscope

Si - Silicon

SiF_6^{2-} - Silicon hexafluoride ion

SiNW – Silicon nanowire

SiNWs – Silicon nanowires

t - oxidation time

t – thickness (Si wafer)

T – temperature in Kelvin

UV - ultraviolet

V_0 - volume of the pre-oxidized SiNW (the volume of the original unoxidized SiNW)

V_1 - total volume of the oxidized SiNW

V_2 - volume of the unoxidized SiNW beneath the oxidation layer

VLS - vapor-liquid-solid

W – watts

X_{ox} - oxide thickness

X_{ox100} - oxide layer thickness aligned to (100) crystal lattice

X_{ox110} - oxide layer thickness aligned to (110) crystal lattice

CHAPTER 1: GENERAL INTRODUCTION

Since their invention in 1990 [1], silicon nanowires (SiNWs) have been a subject of fascination and study by physicists, chemists, engineers and mathematicians. Their unique properties differ from standard bulk silicon (Si) in both quantum [2], [3], [4], [5], [6], [7], [8], [9] and optical [10], [11] band gap. SiNWs are occasionally referred to as "quantum wires," because of these changes in band gap, caused by dimensional confinement.

This thesis is the culmination of several years of fundamental research on SiNWs. Several papers were written, submitted and accepted for publication. There was no direct intent in these studies to find new applications or apply these studies to old applications, but rather, to advance the understanding of the range of fundamental sciences involved in the study of this new and exciting nanotechnology.

In this thesis is discussed the recession of SiNWs, in which it is shown that, based on the concentration of the solution, SiNWs receded into the substrate as they are etched. The degree of recession depends heavily on the concentration. In this study, it was shown that a wide range of recessions can be achieved by variation of the concentration. Additionally, relations are found between the volume of solution and exposed surface area, indicating that the solution is used-up during the etching process.

The study of Si oxidation, because of the extensive use of Si in electronics and computers, has been a subject of great importance for many years. The morphology of SiNWs makes the formulas that describe the oxidation of planar Si [12], [13], [14], [15], [16], [17], [18], [19], [20] inaccurate for describing the oxidation of SiNWs. In this thesis, SiNWs were oxidized and studied, and then mathematical formulae were devised to describe the oxidation of SiNWs.

Surface area calculations were made to show that the area of a Si wafer is greatly amplified when SiNWs are grown on its surface.

The diffusion of dopants into Si is a subject of great importance because of its extensive use in electronics and computers. A great deal of study has been devoted to the study of dopant diffusion [21], [22]. Even greater amount of study has been devoted to the study of diffusion [23], [24], [25], [26], [27], [28], [29], [30], [31], [32], [33], [34], [35] one of the most important and widely used sciences. A small amount of work has been devoted to the study of the doping of SiNWs [36], [37], [38], [39], [40]. In this thesis, a more logical mathematical model is derived for the doping of SiNWs with Boron and Phosphorus. The doping of Si is usually a two-step process, involving first a pre-deposition and then a drive-in oxidation. For each of these steps, the formulae guiding the doping and diffusion of planar Si are different from those guiding the doping and diffusion of SiNWs, because of their morphology. Formulae based on Fick's laws [22], [23] have long been known that apply to cylindrical problems, but have either rarely or not at all been used to describe the doping and diffusion of SiNWs. In this thesis, a set of formulae and a methodology are devised, specifically for the doping and diffusion of SiNWs, based on Fick's laws of diffusion.

Even after a comprehensive study of SiNWs, experiments, studies, research and mathematical expose's much has been learned about the morphology, growth mechanism, recession, oxidation and doping, but one question continues to stand out; h*ow do SiNWs survive the growth process?* The etching process for SiNWs grown by electroless etching of Si has been greatly studied since their discovery/invention, and much is known about the growth process, which is described here in detail (see Chapter 3).

However, the etching process in which SiNWs are produced is ideally suited to etching them into oblivion, yet they survive, and there has yet to be presented a reasonable theory that explains this. Lacking a theory, there is yet to be an experiment to test one.

So this theory will be presented here, so that someday, it can be tested. It is known that only p-type Si can be used with this process (electroless chemical etching with $AgNO_3$/HF) to produce SiNWs. Whenever n-type Si was used, the results did not produce SiNWs, but did etch the surface of the planar Si. The theory here rests on the quantum confinement effect that causes an increase in the band gap of SiNWs. When the band gap is increased, the Fermi energy level shifts in the SiNWs. This shift in the Fermi energy makes SiNWs immune to having electrons taken from them by free Ag ions in the solution at the surface of dimensional confinement (for example, the sides, but not the tips, which undergo recession during etching).

CHAPTER 2: RECESSION AND CHARACTERIZATION OF PATTERNED SILICON NANOWIRES GROWN BY ELECTROLESS ETCHING OF SILICON

Prelude

The material presented in this paper was first presented in Montreal at the 219th Meeting of the Electrochemical Society (ECS) [41]. After the meeting it was published in ECS Transactions [42], becoming part of the meeting record. Subsequent to that it was substantially reworked and accepted as a journal article in the newest ECS Journal of Solid State Science and Technology (JSS), first to be published on July 17th, 2012 [43] and is reprinted here by permission. The material presented in this chapter was part of a larger, long-term study of the fundamental properties of SiNWs in which the newly discovered property of recession was discovered. An extensive study of this recession was made and the results are shown here.

The recession of SiNWs was a heretofore unreported property of SiNWs grown by the electroless process, as was the ability to modulate this recession. The patterning of SiNWs has been done by other groups, but not by the means reported in this paper. The relation of the exposed area to the volume of etching solution and the growth and recession of SiNWs is reported in this paper but has not been previously reported. Since, in previous experiments, there was no reference to determine the depth of the recession and overall etching depth, there has been no previous reporting on the relation of Silver used to Si etched, which is reported in this paper. In this paper, the problem of agglomeration at the tips of SiNWs is discussed at length, but in most other research studies, the agglomeration is barely mentioned, with a few exceptions.

RECESSION AND CHARACTERIZATION OF PATTERNED SILICON NANOWIRES GROWN BY ELECTROLESS ETCHING OF SILICON

R. G. Mertens, K. B. Sundaram
Department of Electrical Engineering and Computer Science

R. G. Blair
Department of Chemistry

University of Central Florida,
Orlando, Florida 32816 U.S.A.

Abstract

Silicon nanowires (SiNWs) were grown by the electroless etching technique using silver nitrate ($AgNO_3$)/hydrofluoric acid (HF) solution on a patterned p-type Silicon (Si) substrate with varying etching times and concentrations. The various etch times and concentrations produced different recession depths wherever the pattern allowed the etching solution to contact the Si substrate. At the bottom of each recession, SiNWs were produced of varying length and size, according to the depth of the recession. In this type of growth procedure, as SiNWs are grown, the tips are etched away. SiNWs grown by this method tend to agglomerate at their tips. We report that the recession and height of SiNWs grown by the electroless process can be controlled directly by the concentration of HF in the etching solution and by the etching time. Under precise conditions, the recession of SiNWs can be very nearly eliminated or nearly complete.

The heights of SiNWs can also be fairly well controlled. We report that the growth of SiNWs is highly dependent on the ratio of volume of etching solution to the exposed surface area.

Introduction

In recent years, SiNWs have drawn an increasingly larger group of investigators, because of their unique properties beyond that of ordinary Si. SiNWs are finding their way into various fields of research and applications, such as solar, chemical sensors, biosensors, and electron devices. SiNWs exhibit quantum confinement which results in a band gap larger than that of bulk Si. Because of this property, SiNWs have found application in various fields, such as solar energy, chemical sensing, biosensing, and other electron devices.

There are many ways to make SiNWs, some of these being vapor-liquid-solid (VLS)[44], [45], chemical vapor deposition (CVD) [46], [47], plasma-enhanced CVD (PECVD) [48], [49] electroless chemical etching [2], [3], [4], [5], [50], [51], [52], [53], [54], E-beam lithography [6], [7] and laser-assisted electrochemical etching [8]. Electroless etching of Si provides a relatively simple means of producing SiNWs for a variety of applications. Probably the most prominent of these is for solar cells, where it has been shown that SiNWs exceed the solar efficiency of bulk Si [9], [55]. Before much more can be done with SiNWs grown in this manner, a great deal more must be known about them, particularly the specific growth mechanisms. SiNWs grown by electroless etching are much less expensive to make than by other methods.

There are two significant advantages of applying SiNWs to solar cell technologies. The first of these is known as quantum confinement, which causes an increase in the band gap energy. This is often referred to as the “blue shift,” effect [2], [3], [4], [5], [6], [7], [8], [9]. In the blue shift, the band gap of the material, in this case, Si, can be significantly increased. The

band gap of bulk Si of 1.1 eV can be changed to as high as 2.5 eV, additionally, from an indirect band gap to a direct band gap as a result of the dimensional confinement. This effect was most readily discernible in early observations of visible photoluminescence with porous Si [4], [8]. SiNWs that are carefully sized can be tuned for a band gap of 1.4-1.5 eV, which can shift the photoresponse of Si closer to the typical solar irradiance of air mass 1.5 (AM1.5) [56] , thereby improving the external quantum efficiency [57] and therefore, the energy collection ability of solar cells. SiNWs produced by electroless etching do *not* exhibit discernible, visible photoluminescence when exposed to low-power sources (less than 100W) of ultraviolet (UV) light at 254nm and 365nm wavelengths. The reason for this is that SiNWs produced by this method are too large to undergo a substantial quantum confinement, which only takes effect once SiNWs approach 10-15nm in width [58]. A second advantage of SiNWs is that they are highly absorptive of light. Regular, polished Si is 20 to 40% reflective (depending on wavelength), while SiNWs are only about 4% reflective [45]. Antireflective (AR) coatings must be applied to modern solar cells in order to improve cell efficiency and reduce reflectance. An unfortunate effect of SiNWs is that the space between them is smaller than the shortest wavelengths (~380nm) of visible light. Even so, SiNWs are still fairly dark, and most of the light striking them is absorbed.

Lately, SiNWs are being applied to biosensor technologies, especially gene detection [59], [60], [61], [62]. This brings SiNWs into a new arena of biotechnology not before seen and lends them a value beyond measure, opening up a wide array of biomedical, chemical, industrial, and many other sensing applications.

Growth Mechanism

Silver is precipitated, in the form of silver dendrites, in this etching process, which terminates with its depletion in the solution, and the sample, typically coated in a thick blanket of silver dendrites. While there has been some debate about the etching process itself [50], [52], [53], [63], [64], some parts of it are not in question. For one thing, it is accepted that silver (Ag^+) ions in the solution attach to the surface of the bulk Si and remove an electron from it, thereby leaving unattached or dangling Si bonds. The precipitated silver subsequently attracts other silver ions, which attach either to it or to the surface of the bulk Si to form dendrites, in random patterns.

SiNWs are formed in the reaction:

$$Ag^+ + e^- \rightarrow Ag \tag{2.1}$$

$$Si + 6F^- \rightarrow SiF_6^{2-} + 4e^- \tag{2.2}$$

where the global chemical reaction is:

$$4Ag^+(aq) + Si^0(s) + 6F^-(aq) \rightarrow 4Ag(s) + SiF_6^{2-}(aq) \tag{2.3}$$

Electrons from four silver atoms are captured from each Si atom beneath the silver nucleation sites. Silver does not cap the SiNWs, but rather, drops down between the SiNWs in pits and provides the necessary electrons to etch downward even further, leaving the SiNWs (mostly) untouched, while providing an attractive nucleation site for silver ions in solution.

Experiments with H_2O_2 and HF [63], using an evaporated silver layer to show that, with a 20nm layer, the same SiNWs produced by the $AgNO_3$-HF process can be very nearly duplicated by this process. They show that, in very short etching runs (15s), the silver sinks into the Si.

Similar experiments [64] with silver and gold evaporated onto Si prepared with randomly scattered polystyrene spheres produced SiNWs under the spheres, showing that the etching took place directly underneath the gold or silver films.

The dendrites that grow during this process are shown to be pure silver [65]. This suggests that, as the dendrites grow, they carry no additional solid matter with them, nor do other atoms interlace with the silver. Since the Si surface must recede before the silver dendrite trees, it is reasonable to suggest that the dendrites must grow, if not completely from the bottom down, then at least partially, filling the space between the existing dendrite tree and the receding Si surface beneath it. Scanning electron microscope (SEM) evidence of silver particles, confirmed by energy-dispersive X-ray spectroscopy (EDS) study [65], in the pores at the bottom of the SiNWs demonstrate that the etching takes place between the SiNWs.

The lengths of the SiNWs are directly related to the amount of silver in the solution and the amount of Si that must be removed in order to produce the SiNWs. It is expected that at least four silver atoms must be precipitated in order to release one atom of Si from the bulk crystal lattice.

Recession of SiNWs

When SiNWs are made, the etching process begins at the surface of the substrate, etching downward along crystal alignments. SiNWs begin to form immediately, but as the etching proceeds further into the substrate, the tops of the SiNWs are etched away, as shown in Figure 1A. In order to measure this recession, a surface separate from the etched substrate must be protected against etching, for a means of comparison (of etched to non-etched material). To do this, photoresist (PR) was applied to the surface of the substrate, a photomask was used to define

the regions, as shown in Figure 1B. Using this method, undercutting is expected, depending on the depth of the recession.

There has been no systematic reporting on the recession or calculation of recession of SiNWs grown by the electroless process, on the basis of growth times or concentration of solution. This paper also discusses methods of controlling the heights of SiNWs. These are essential elements in understanding the growth mechanisms of SiNWs made by the electroless process.

Experimental Procedure

All of the SiNWs samples were prepared in Class 1000, or better, clean room conditions. Single-side polished, p-type (100) Si wafers (resistivity, $\rho = 5 – 50\ \Omega$-cm, $t = 705.0 – 745.0\ \mu$m) were cut into squares 2.54cm by 2.54cm. The samples were cleaned with acetone, methanol and rinsed with deionized (DI) H_2O. The wafers were N_2 blow-dried, dipped in a standard buffered oxide etch (BOE) solution with HF for one minute, rinsed in DI H_2O and N_2 blow-dried.

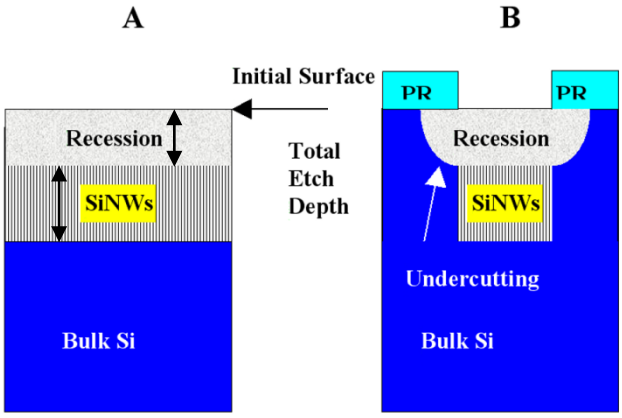

Figure 1. A. Recession during SiNWs preparation and B. Recession and undercutting in a patterned sample using a mask.

The following PR process was performed in a Class 100 clean room: Both polished and unpolished sides were coated with negative PR. The purpose of the PR on the unpolished side of each wafer was to prevent SiNWs growth. A patterned mask was placed in the mask aligner and the polished side of each wafer was exposed for 10 sec. A blank mask was used for the unpolished side of each wafer. All of the wafers were developed and inspected to verify pattern development. Each wafer was hard-baked at 150°C.

Growth of SiNWs

Normally the samples are etched in a solution of 20% 0.1 M $AgNO_3$, 20% of 49% HF (by weight) and 60% DI H_2O for 45 minutes at room temperature (20°C). In this experiment, HF concentrations of 11, 16, 20 and 24% HF (by volume) in the solution were used, as shown in Tables 1, for etch times of 5, 15, 30 and 45 min. The etch times and ratios for each sample are shown in Table 2. In Tables 1 and 2, the concentration of HF refers to percentage of 49% solution. Post-etching treatment is essential for good results.

Table 1 Concentrations

Samp#	1-4	5-8	9-12	13-16
Ratio HF	11%	16%	20%	24%
$AgNO_3$ (ml)	6.7	6.3	6	5.7
HF (ml)	3.3	4.8	6	7.1
H_2O (ml)	20	18.9	18	17.2
Tot (ml)	30	30	30	30
Mass Ag (mg)	72.3	68.0	64.7	61.5

The SiNWs are extremely delicate and are easily ruined, broken or destroyed. During the etching process, a blanket of silver dendrites grows over the region wherever etching is taking place [66]. The samples were removed from the etching solution, rinsed with DI H_2O, which

removes the silver dendrite blanket by spray pressure. Any remaining silver was removed subsequently with a dip in 25% dilute HNO_3, followed by DI H_2O rinse and N_2 blow-dry. After completion of this step, occasionally, some silver remains, which is removed by a 2-min. dip in BOE, followed by a DI H_2O rinse, then N_2 blow-dried

Table 2 HF Concentration Ratios and Etch Times

Ratio HF	11%	16%	20%	24%	Etch time
Samp #	1	5	9	13	5 min
Samp #	2	6	10	14	15 min
Samp #	3	7	11	15	30 min
Samp #	4	8	12	16	45 min

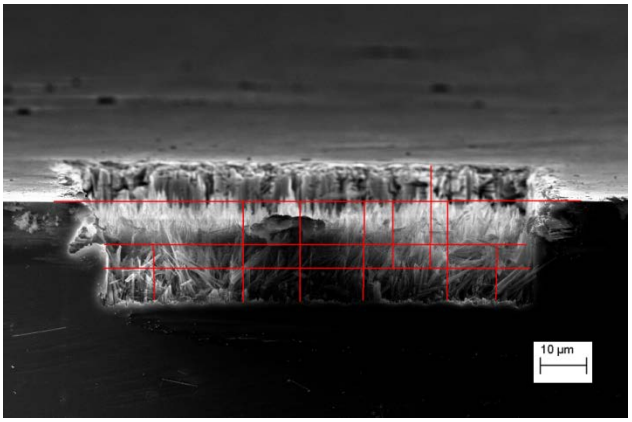

Figure 2. SiNWs heights were measured using SEM techniques and image analysis software. Cross-hatch lines were used for the measurements.

Measurement of SiNWs heights was made through scanning electron microscopy (SEM) techniques, using a Zeiss Ultra55. Image measurement/analysis software (JMicroVision) was used to measure the heights of the SiNWs, the depth of the overall etch, and/or the recession of the SiNWs (two or three of these can be measured in order to get all three values), as shown Figure 2. Image measurement/software traces (grid lines) were used to make measurements, using the SEM reference line for the spatial calibration.

Results and Discussion

For the 11% solution, measurements showed a maximum SiNWs height of 2.5μm, with a maximum etch depth of 16μm, showing that SiNWs receded into the bulk Si a maximum of 13.5μm. SiNWs were clumpy, sparse and inconsistent in height, while the walls around the edge of the pattern were roughly cut and etched into, as observed in Figure 3.

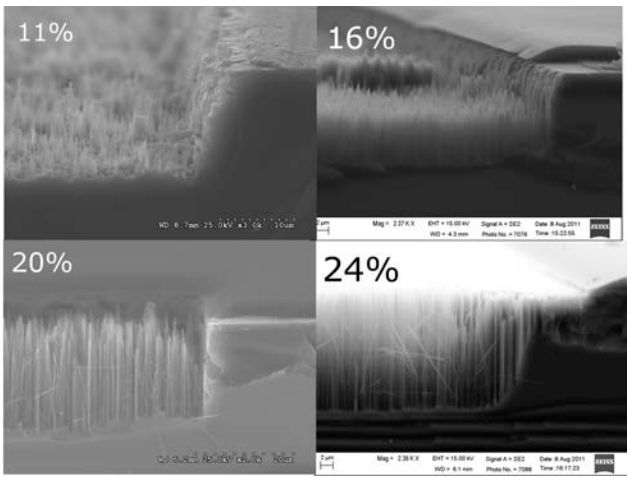

Figure 3. Data were collected from SEM images taken of SiNWs grown in HF solutions of 11, 16, 20 and 24%. A very low concentration yielded very small SiNWs with a deep recession, while high concentration yielded very tall SiNWs with almost no recession.

Figure 4 shows the etch depth and recession as a function of etching solution concentrations and etch times. From Figure 4(a), it is clear that the recession was fairly continuous, so that any SiNWs grown in the first 40 minutes were completely etched away. What remains are SiNWs that were grown in the last five minutes. It is apparent, however, that the first five minutes of etching do not equal the last five minutes. As the etching proceeds, the growth morphology of the SiNWs depends heavily on the existing morphology. SiNWs are built and shaped from existing structures and they evolve, grow and dissolve. In the formation of the

SiNWs, there is no agglomeration, typical in the growth of longer SiNWs. Only sharp, isolated spires remain after the etching cycle is completed.

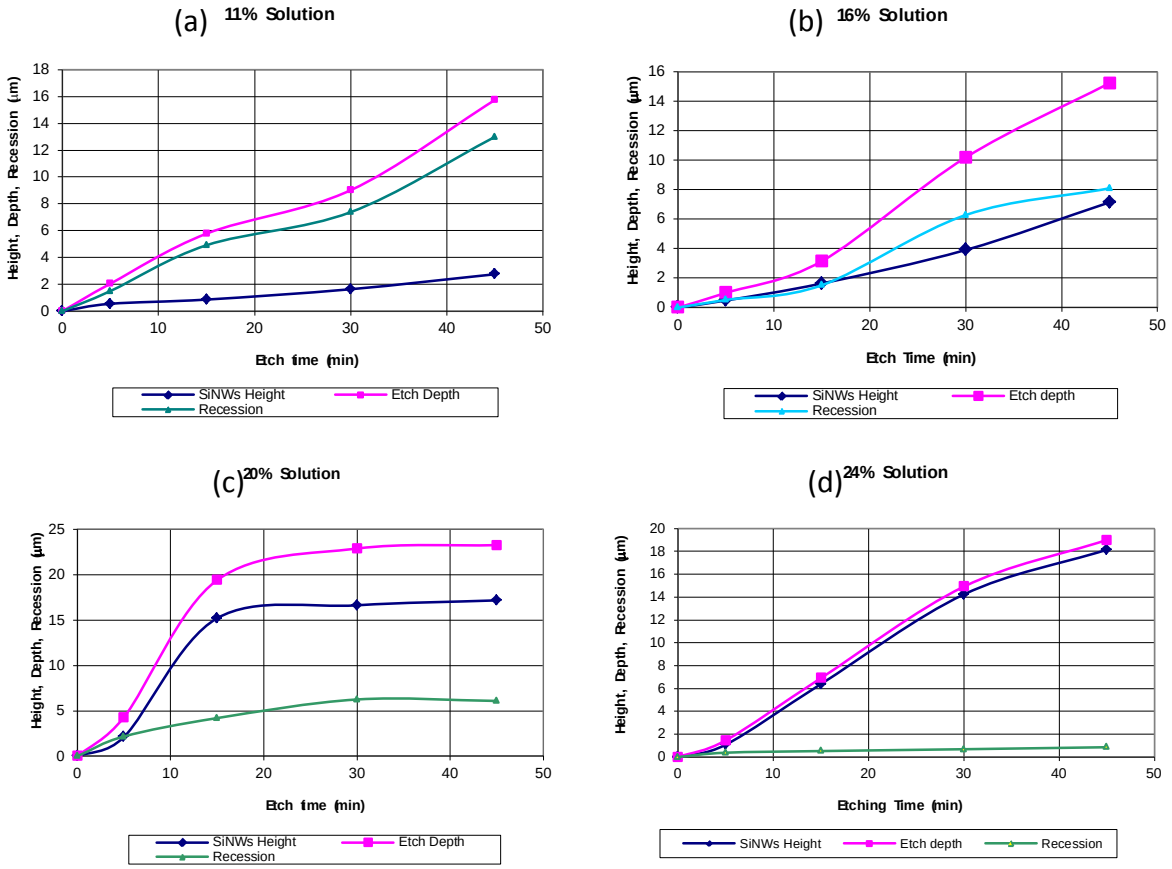

Figure 4. SiNWs height, etch depth and recession as functions of etching time, with solutions of (a) 11%, (b) 16%, (c) 20% and (d) 24% for 5, 15, 30 and 45 minutes.

For the 16% solution, shown in Figure 4(b), measurements showed a maximum SiNWs height of 7µm, with a maximum etch depth of 15µm, showing that SiNWs receded into the bulk Si a maximum of 8µm. The results of this experiment show fairly consistent SiNWs heights and less etching into the walls around the edge of the pattern, as observed in Figure 3. The PR along

the edge of the pattern is also in better condition, although undercutting is apparent. From the graph of Figure 4(b), it is plain that the recession was fairly continuous, so that any SiNWs grown in the first 25 minutes were completely etched away. What remains are SiNWs that were grown in the last 20 minutes. Again, these are heavily dependent on the existing morphology, as SiNWs evolve, grow and dissolve. These SiNWs show few signs of agglomeration, forming primarily as spire-like structures.

For the 20% solution, shown in Figure 4(c), which is the typical solution for this experiment, measurements showed a maximum SiNWs height of 17μm, with a maximum etch depth of 23μm, showing that SiNWs receded into the bulk Si a maximum of 6μm. Generally, these are considered to be the "best" results, this being a commonly used concentration [50], [52], [53], [54], but this depends upon what the ideal is expected to be for the application. SiNWs are well-aligned, vertical and exhibit the typical morphology, as seen in Figure 3. There is some undercutting in the PR, but the side walls of the pattern appear to be relatively untouched. From Figure 4(c), it is plain that the recession was fairly discontinuous, so that only SiNWs grown in the first seven minutes were completely etched away. What remains are SiNWs that were grown in the last 38 minutes. Again, growth evolution is dependent on the morphology of the existing structures, although in this case, SiNWs appear to grow out and away from agglomerations around the tips of the structures.

For the 24% solution, shown in Figure 4(d), measurements showed a maximum SiNWs height of 18μm, with a maximum etch depth of 19μm, showing that SiNWs receded into the bulk Si a maximum of 1μm. This experiment exhibited the least amount of recession, which was in fact, barely detectable in the images, as shown in Figure 3. The SiNWs in this experiment were tall as well – taller than in any of the other experiments. However, the etch depth was less than

with the 20% solution, indicating that the 24% solution was a bit more efficient at producing tall SiNWs. From Figure 4(d), it is plain that the recession was very limited, so that any SiNWs grown in the first three minutes were etched away. What remains are SiNWs that were grown in the last 42 minutes. Growth evolution was heavily dependent on existing morphology, as with the 20% group, agglomerating at the tips and growing outward and away from them.

Relation of Exposed Surface Area to Volume of Etching Solution

In the production of the dendrite blanket, silver is consumed so that the same solution cannot be used a second time for the same process on a new sample. From this piece of data and the graph of the 20% solution in Figure 4(c), we can see that the etching process stops after consumption of all of the silver. In this graph, it occurred in about 30 minutes. For the graph of the 24% solution in Figure 4(d), etching was incomplete since the curve is not flattened at its termination. The curve showing the etch depth is still pitched upward at its tail.

In previous experiments, typical SiNWs heights were around 4μm, and these also completed in about 30-45 minutes. However, after a new method was engaged, that of protecting the bottoms of the samples with PR, SiNWs heights increased, suggesting that the heights of SiNWs has a correlation with the area being etched. This intermediate step was adopted for all subsequent experiments. With the addition of patterning to the etching process, a substantial area of the sample was protected from etching, thus magnifying the heights to six-fold (24μm) the previous results. Estimating that the exposed area with a pattern has been reduced to approximately 5% of its previous coverage (half of that if the bottom of the sample is also protected), we expect a 20-fold increase (80μm), which does not occur. We therefore conclude that this is a non-linear relationship.

In this calculation we ignore the bottom of the wafer. The bottom half, if left unprotected, etches somewhat, but not nearly as much as the top half does, since the bottom is in contact with the bottom of the etching container, thereby preventing the solution from circulating and thus providing much needed silver for the etching process. In this case, the initial growth of silver dendrites act as a blanket, preventing the circulation of solution. Protecting the bottom half of the wafer with PR prior to etching prevents this random process from interfering with these calculations.

Relation of Silver Used to Silicon Removed

It is desirable to know how much Si was removed in relation to the amount of silver that was precipitated, thereby giving an indication somewhat whether the chemical formulas above have validity. In general, when this process is used, it is easier to determine this if a pattern of known dimensions is used, thereby giving the depth of etching, and the amount of material removed. The standard solution, given in Table 1, is 20% of 49% HF, and 20% of 0.1M $AgNO_3$ (60% DI H_2O). This experiment uses 30ml at a time, which yield 64.7mg of silver in the 6ml out of this solution. For the other concentrations of 5.7ml, 6.3ml, and 6.7ml the calculations are shown in Table 1.

During this experiment, with the standard solution, the total etch depth was 23.253μm and the SiNWs height was 17.166μm. The total area of the sample was 2.54cm x 2.54cm (one square inch), or 6.452cm^2. The bottom of the sample was protected from etching by PR. The exposed area of the top of the sample is calculated to be 4.93% of the total area, or 0.32258cm^2. From Shiu, et. al. [67], we get the number of $3x10^7$ SiNWs/mm^2. From measurements of several hundred SEM images (data collected from many previous experiments), we calculated an

average SiNWs diameter of 56.6nm. The calculated volume of the SiNWs is negligible compared to the volume based on the area and the etch depth, so the volume of the SiNWs was ignored in this calculation. With these data we calculate the mass of the etched Si to be 1.723mg. Using the molar masses 107.868 and 28.085 for silver and Si, respectively, we obtain an atomic ratio of 9.78:1 of Ag:Si. This is roughly a 10 to one ratio of atoms.

Four of these silver atoms are used up in etching Si. The other 5.78 atoms might be doing other reactions. Ammoniacal silver solutions are known as Tollen's reagent. In the presence of an aldehyde (a chemical reductant) Ag+ is reduced to Ag(0), however, other side reactions occur that result in the production of Ag_2O and AgOH

$$H_2O \rightarrow H^+ + OH^- \tag{2.4}$$

$$Ag^+ + OH^- \rightarrow AgOH(s) \tag{2.5}$$

and/or

$$2Ag^+ + 2OH^- \rightarrow Ag_2O(s) + H_2O \tag{2.6}$$

$$2H^+ + 2e^- \rightarrow H_2 \tag{2.7}$$

It usually looks like a brown-black sludge. We have observed similar by-products in our experiments (Figure 5A). When the silver dendrites are dried in air and viewed under a microscope, they have an appearance not too unlike snowflakes, as shown in Figure 5B. In this image, a very close inspection will reveal the presence of brownish tinged spots in amongst the dendrites, suggesting the presence of of Ag_2O and AgOH.

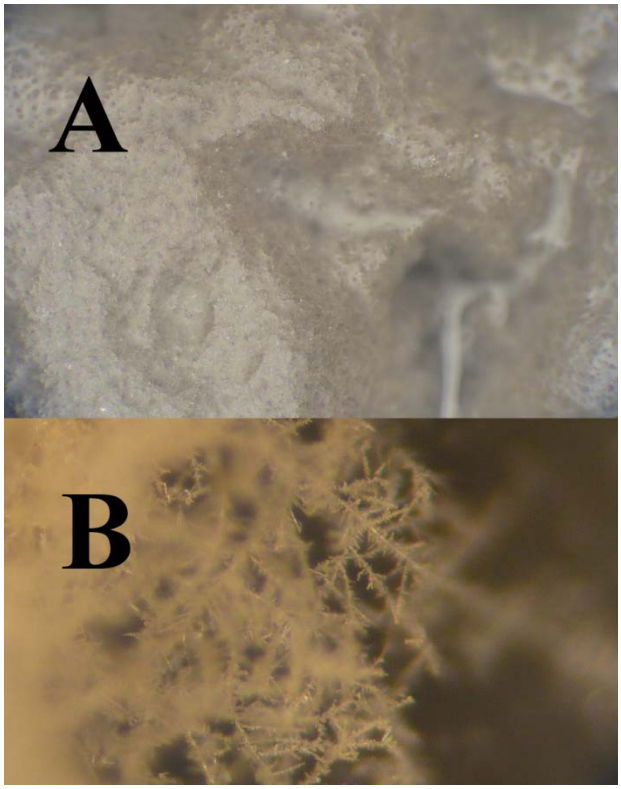

Figure 5. A. Silver dendrites still wet after etching and removal have the macroscopic appearance of brown sludge. B. Dried silver dendrites viewed under a microscope. A brownish tinge suggests the presence of Ag_2O and AgOH.

Comparison of the SiNWs Etched in Various Concentrations of HF

Figure 6 shows the effect of HF concentration on the recession. It is clear that as the solution concentration increases, the recession decreases, in general, although this only works within limits, since in all cases, the other precursors must be present in some degree. Taller SiNWs can be achieved with higher concentrations of HF, as seen from the graph. With 20% concentration, the etch depth is increased, as is the recession. From this graph, it seems apparent that the 45-minute etch cycle is insufficient for the 24% concentration. From Figure 4, comparing the two graphs of the 20 and 24% concentrations, the 20% concentration levels off

after 30 minutes of etching, while the 24% solution is still rising, but appears to be near a leveling-off point. This suggests that the increased concentration of HF in the solution may be extending the usefulness of the silver in the solution.

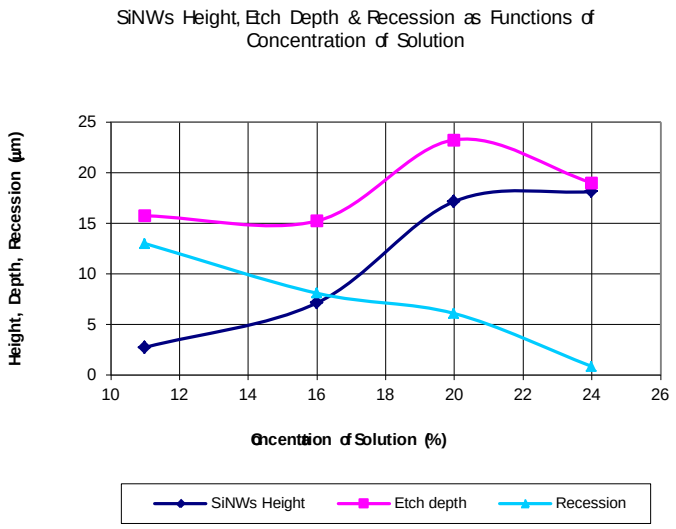

Figure 6. A graph showing the heights of SiNWs grown in 11%, 16%, 20% and 24% solution for 45 minutes, also giving the total etch depths, with the recession as a result.

Agglomeration at the Tops of SiNWs

In spite of the unique and powerful properties of SiNWs, there are some obvious and recognizable drawbacks to this specific type of SiNWs. One major drawback is the agglomeration of SiNWs that occurs at the tips, as shown in Figure 7. This is an apparent and seemingly unavoidable consequence of the method of growth (excepting when the concentration of HF is changed, but these solutions produce SiNWs that are very short). Another drawback is the inconsistency of sizes and shapes in the SiNWs. We find in our studies that the average width of SiNWs is about 100nm. These also exhibit some ribbon-like shapes in some places.

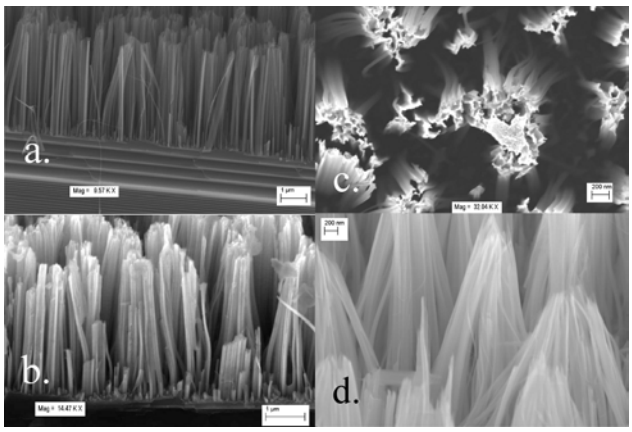

Figure 7. a. SEM edge-on view of SiNWs, b. SEM edge-on view of SiNWs that were oxidized, c. SEM top view of SiNWs, d. SEM edge-on view of SiNWs after oxidation and oxide etch.

The agglomeration of SiNWs at the tips is mostly attributed to van der Waals forces. Kumar, et. al. [65] observe this for SiNWs beyond a certain height. However, they do not state, at which length of SiNWs this occurs or begins to occur. Silverberg [68] takes this a step further, in an experiment unrelated to SiNWs, but with metal nanowires (NWs) instead. In his experiment, vertical, aligned, cylindrical NWs are electrodeposited in an alumina template. When the template is removed, the NWs agglomerate at their tips. This agglomeration (clumping) is attributed to van der Waals forces.

This agglomeration has been observed (under SEM) at all observed intervals (5, 10, 15, 30 and 45 minutes) during the growth process. It is additionally observed at various concentrations of the chemical agents used in the growth process, with the exception of concentrations of HF of 11% or less. Agglomeration also remains after SiNWs have been partially oxidized and subsequently etched.

As a result of agglomeration of the SiNWs, there is a great deal of area that is unreachable by many traditional methods of contact material deposition. There are, almost

invariably, no single strands of SiNWs at a tip, and a minimum of perhaps four or five SiNWs per agglomeration. Additionally, many agglomerations are connected to other agglomerations, in strings of agglomerations.

Conclusion

It is advantageous to be able to control the size, regularity and pitch of SiNWs, which has been done by masking with silica colloidal nanoparticles [54] in large dimensioned (relatively speaking) arrays. From this point, a closer examination of precisely sized SiNWs can lead to a better set of guiding equations for the oxidation of SiNWs. We derive some conclusions inherent in the outcome of this and other experiments, first, that SiNWs do recede into the substrate as they are grown and that the recession of SiNWs is dependent on several factors, large among these being the etching time and the concentration of HF in the etching solution.

Another factor is the ratio of exposed Si area (area unprotected by PR) to the volume of solution. This factor became apparent after a number of experiments in which a very small amount of exposed area yielded SiNWs heights of up to 26μm, whereas typical results had been around 3-5μm with large exposed areas (including the bottom). The greater part of this discussion is the consumption of silver in the etching process. As the SiNWs are produced (the bulk Si is etched), the silver dendrite blanket forms, made from silver, which is then ejected or grown from the etching site. When the silver in the solution is depleted, the etching process ceases.

When Si is etched around patterns, the silver dendrites no longer occur as a "blanket," covering the entire sample, but as "strings," or "stacks" growing and emerging from each of the patterns, and from the holes in the patterns as the etching progresses down into the substrate.

The height and recession of the SiNWs can be modulated, which means that the tops can be cut off to any degree desired via the etch concentration.

Finally, we conclude that the concentration of HF in the etching solution can produce very large variations in the recession of SiNWs. With a sufficiently small concentration of HF in the solution, the ratio of recession to SiNWs height can be 20:1 or more, while with larger concentrations, this ratio is about reversed to as much as 1:20.

CHAPTER 3: MATHEMATICAL CHARACTERIZATION OF OXIDIZED CRYSTALLINE SILICON NANOWIRES GROWN BY ELECTROLESS PROCESS

Prelude

In the study of SiNWs, probably one of the first aspects one might wish to study is their oxidation, since oxidation is such a large part of the semiconductor process in the manufacturing sector, and certainly a big part of the semiconductor learning and education process. The oxidation of Si has a long and well-studied history, with the evolution of many formulae relating to oxidizing of planar Si, but very little in the way of SiNWs. Oxidation of Si is both a chemical and a diffusion process, giving it complexity well beyond that of ordinary diffusion processes and mechanisms.

One of the main purposes of the oxidation of Si is to block diffusion of dopants into areas where doping is not wanted. This process is rendered impractical when applied to SiNWs, because the thickness of oxidation needed to block doping, in most cases, is much greater than the diameters of the SiNWs. However, there are many other aspects of oxidation of SiNWs that do make this study important. This study is part of a larger study on the properties of SiNWs. A number of other research groups have studied the oxidation of SiNWs, although this number is small. A somewhat smaller number has made a good deal of effort to mathematically describe the oxidation of SiNWs. Some software groups have made numerical models for moving boundary problems unrelated directly to the oxidation of SiNWs, but useful in the application to this problem.

While the study of cylindrical oxidation has been studied, and figures similar to the ones found in this article appear in other journal publications, all of those deal only with relatively large-scale (micron) cylindrical oxidation, and do not deal with the oxidation formulae of the very small-scale (nanometer) cylindrical oxidation. Since SiNWs made by the electroless process used here are so close together, this is a subject of limitation not discussed in other publications. Only one other publication has discussed the density of SiNWs made by the electroless process, and have done so by a legitimate and repeatable process, so that has allowed an opportunity to build on this knowledge, which was heretofore not discussed.

This material was published in Elsevier's Appled Surface Science [66] and is reproduced here by permission.

MATHEMATICAL CHARACTERIZATION OF OXIDIZED CRYSTALLINE SILICON NANOWIRES GROWN BY ELECTROLESS PROCESS

Robert G. Mertens[1], Kalpathy B. Sundaram
School of Electrical and Computer Engineering
University of Central Florida, Orlando, Florida 32816 U.S.A.

Abstract

Silicon nanowires were created via the electroless etching technique using silver nitrate ($AgNO_3$)/hydrofluoric acid (HF) solution. The prepared raw samples were oxidized for various intervals, so as to have an end result of various nanowire thicknesses. Scanning electron microscope (SEM) images were taken of the original nanowires, the oxidized nanowires and then the oxidized and etched (in HF solution) nanowires. When Silicon nanowires are made, the area of exposed Silicon undergoes "amplification," a formula for which is provided herein. When Silicon nanowires are oxidized, the growth rate of the oxide layer varies according to the crystalline alignment. A formula for a polar plot is provided for illustrating the shape of a Silicon nanowire after oxidation for various intervals, based on the Deal-Grove and Massoud models of oxidation.

Keywords: Silicon, nanowires, oxidation, orientation.

[1] Corresponding author 19 (407) 893-6497 quarkmaster@gmail.com

Introduction

Silicon nanowires (SiNWs) have yet to find a place in the market, and at this time, remain an intellectual and experimental curiosity. There is growing interest in applying this technology to a wide variety of technologies, probably the most prominent of which is solar cells. The popularity and inexpensive production costs of polysilicon solar cells has supplanted the use of other technologies, in spite of its low efficiency [69]. SiNWs grown by etching are much less expensive to make than by other methods, such as vapor-liquid-solid (VLS) and chemical vapor deposition (CVD) [50], [51], [52], [53], [54], [2], [3], [4], [55].

There are a number of advantages of applying SiNWs to solar technologies. The first of these is known as the quantum confinement or, "blue shift,"
effect [70], [71], [72], [73], [1], [74], [75], [76]. In the blue shift, the band gap of the material, in this case, silicon, is increased. The original band gap of bulk silicon can be changed to as high as 2.5 eV, additionally, from an indirect band gap to a direct band gap as a result of the dimensional confinement. This effect was most readily apparent in early observations of visible photoluminescence with porous Silicon [72], [73], [1], [74], [75]. The outcome of this is to shift the photoresponse of silicon closer to the solar output at the earth's surface, thereby improving the energy collection efficiency of the cell.

Another advantage of SiNWs is that they are highly absorptive of light. Regular silicon is 20 to 40% reflective (depending on wavelength), while SiNWs are only about 4% reflective2. Antireflective (AR) coatings must be applied to solar cells in order to improve cell efficiency and reduce reflectance. An unfortunate effect of SiNWs is that the space between them is smaller than the shortest wavelengths of ordinary light. Even so, SiNWs are still fairly dark, and most of

the light striking them is absorbed. Yet another advantage of SiNWs is the high surface area. Until recently, there was no reliable means to determine the number of SiNWs per unit area that were made by this process. Shiu, et. al. [67] were able to transfer SiNWs from the substrate to the surface of a transparent substrate, resulting in flipping the SiNWs upside-down, thus allowing, for the first time, for the SiNWs to be counted with some degree of accuracy. The peak transfer of SiNWs achieved was $3 \times 10^7/mm^2$. This number can be taken as a minimum value, since this was not the maximum number of SiNWs that could be transferred.

Material and Methods

Growth of Silicon Nanowires

All preparations were carried out in a Class 1000 or 100 clean room. Boron-doped p-type (100) CZ silicon wafers with resistivity $\rho = 5 – 50\ \Omega$-cm, were cut into squares about 2.5 x 2.5 cm. The wafers were cleaned with acetone, methanol and rinsed with deionized (DI) H_2O. This was followed by a dip in a standard buffered oxide etch (BOE) solution of HF for one minute, rinsed in DI H_2O and N_2 blow-dried. The wafers were etched in a solution of 20% 0.1 M $AgNO_3$, 20% by 49% HF (by mass) and 60% DI H_2O for 45 minutes at room temperature.

During this procedure the following were observed; the samples became stained immediately on contact with the etching solution and after about ten minutes of etching, a growth of silver dendrites was observed on each sample, as shown in Figure 8a. Post-etching treatment is essential for good results. The SiNWs are extremely delicate and are easily ruined, removed or destroyed. The first step after etching was the essential removal of the silver dendrite blanket, which was done with a DI water rinse, as shown in Figure 8b. The Silver dendrite blanket can

also be removed with nitric acid (HNO_3), but this method causes substantial damage to the SiNWs. The samples were dipped in 25% HNO_3 until black in the solution[2], rinsed with DI H_2O, second dipped in 25% HNO_3, rinsed with DI H_2O again and N_2 blow-dried. The silver dendrites, viewed under a microscope have a snowflake-like appearance, as shown in Figure 8c.

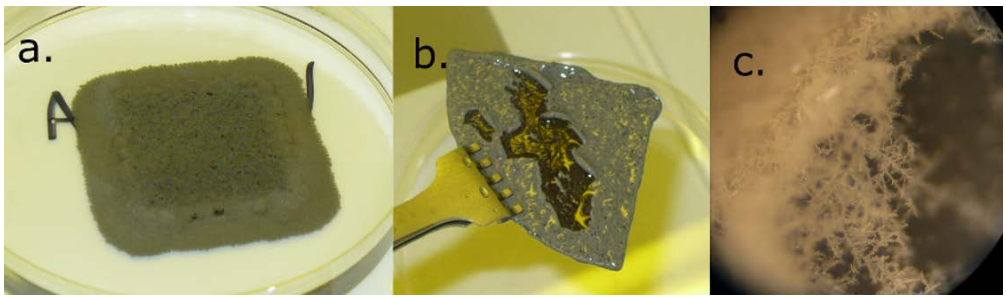

Figure 8. Silver dendrites a. growing in the solution, b. being rinsed away following etching and c. under the microscope.

SEM Examination

After the cleaning and silver removal process was completed, the SiNWs were viewed in a Zeiss Ultra 55 SEM, obtaining Figure 10, a sample prior to oxidation. SiNWs in this image are 3.8 μm in height, with an average width of 65 nm. The greatest measured width was 103 nm and the thinnest was measured to be 35 nm. On other samples, the heights and widths varied according to a number of parameters that are generally associated with the precursors for the etching process, including the concentrations of solutions, amount of solution per unit area and so on.

[2] After removal of the dendrites, the wafer and the SiNWs take on a greenish-brown hue, the appearance of which is caused by leftover silver dendrites in, on and around the SiNWs. In early experiments, this was generally taken as "a few minutes" or until the wafer had turned black. In later experiments, this time was set to a consistent value of ten minutes, and removal of the second HNO_3 step. An additional step to cleanse the wafer of any remaining heavy metals is a two-minute BOE following a thorough DI H_2O rinse after the HNO_3 dip.

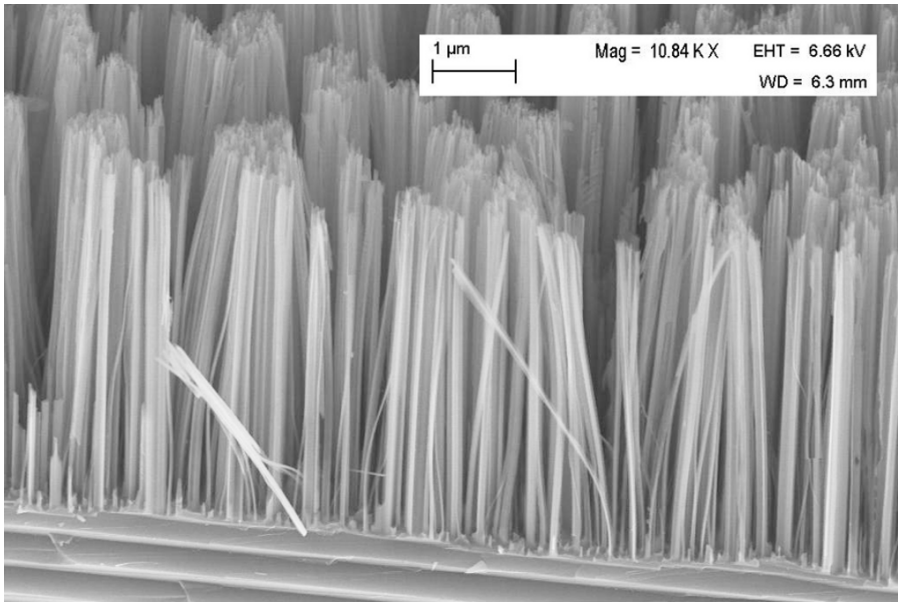

Figure 9. SiNWs grown on p-type (100) Si using electroless process in AgNO3/HF solution for 45 minutes.

Oxidation and Etching of Silicon Nanowires

The dry oxidation took place at 900°C, according to Table 3, where Samples a and b were oxidized for 20 minutes, Samples c and d were oxidized for 40 minutes and Samples e and f were oxidized for 60 minutes, each with target push-in and pull-out times of one minute. Sample 1 was not oxidized. Samples b, d and f were etched in standard BOE for one minute (the BOE etch rate was 600Å/min.). Visual observation showed the SiNWs to still be in place.

Table 3 Experimental Oxidation & Etching Settings

Sample #	Experiment Settings		
	Oxidation Time (min)	BOE Etch Time (min)	Figure
1	0	0	2
a	20	0	3a
b	20	1	3b
c	40	0	3c
d	40	1	3d
e	60	0	3e
f	60	1	3f

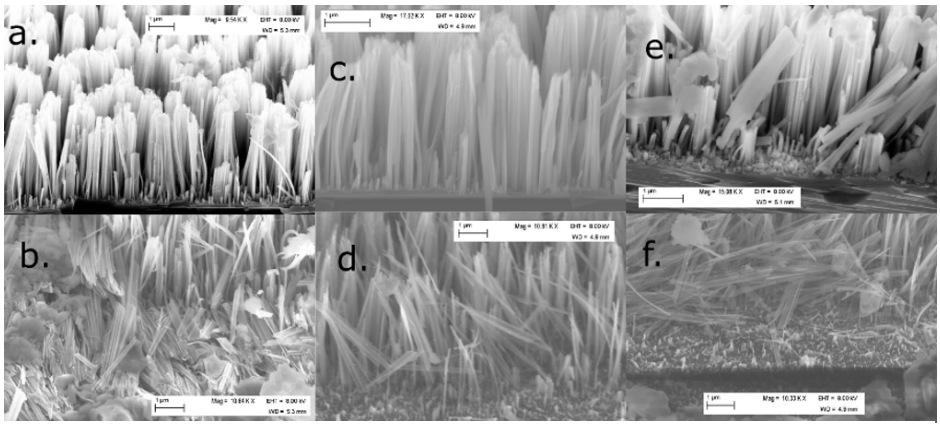

Figure 10. a, c & e after oxidation and b, d & f after oxidation and etching in BOE for one min. Samples a & b oxidized for 20 min, Samples c & d oxidized for 40 min and Samples e & f oxidized for 60 min.

Cleaving, Sonication and Separation of SiNWs

Samples a-f were cleaved for examination under the scanning electron microscope (SEM). Pieces from samples b, d and f not placed under the SEM were sonicated for 60 min. in Methanol. The result of sonication is that SiNWs break away from the substrate and go into suspension. The sonicated samples were held in suspension for examination under the TEM.

Theory and Calculations

Surface Area Calculations

From the work of Shiu, et. al. [67], various assumptions can be made about the lengths and widths, and the total surface area can be calculated. It is assumed that, during the process of etching, the bottom of the wafer is protected from etching, so that the calculation is not confused by partial etching of the bottom of the wafer. Only the top of the wafer is considered in the total area calculation.

$$A_T = A_W + A_{NW} N_{NW} \tag{3.1}$$

where A_T is the total area, A_W is the area of the wafer, A_{NW} is the area of a single SiNW and N_{NW} is the total number of SiNWs on the wafer. Each of these were computed as follows;

$$A_{NW} = d_{NW} \pi H_{NW} \tag{3.2}$$

where d_{NW} is the average diameter and H_{NW} is the average height of the SiNWs.

$$N_{NW} = n_{NW} A_W \tag{3.3}$$

where n_{NW} is the average number is SiNWs per unit area. Putting these three equations together, we obtain an equation for the total area of a wafer with SiNWs;

$$A_T = A_W \left(1 + d_{NW} \pi H_{NW} n_{NW}\right) \tag{3.4}$$

From this equation, a factor can be devised as an amplification of area, or the area amplification factor, A_F, that is the result of creating SiNWs on a silicon wafer of any area. This varies according to the height, diameter and number of SiNWs per unit area, all of which vary according to a number of key factors during the process of making SiNWs. The area

amplification factor is the ratio of total area of silicon (including the SiNWs) to the pre-etch (excluding SiNWs) wafer area. This is written as:

$$A_F = \frac{A_T}{A_W} = \frac{A_W\left(1 + d_{NW}\pi H_{NW} n_{NW}\right)}{A_W} = 1 + d_{NW}\pi H_{NW} n_{NW} \tag{3.5}$$

For $A_F >> 1$, we get the simplified formula:

$$A_F = d_{NW}\pi H_{NW} n_{NW} \tag{3.6}$$

Assuming that the average radius of a SiNW is 35 nm (given the average diameter of 70 nm) and that the minimum number of SiNWs per square mm is given by Shui, et. al. [67] to be $n_{NW} = 3 \times 10^7/mm^2$, but could be potentially much higher, conservatively guessed at $n_{NW} = 7 \times 10^7/mm^2$, this amplification factor, A_F, is graphed in Figure 11, according to the average height of the SiNWs grown, which, depending on the process, vary between 1 μm and 70 μm [77].

Rewriting Eq. 3.3 as

$$n_{NW} = \frac{N_{NW}}{A_W} \tag{3.7}$$

Using Figure 12 as a guide, if the total area of the wafer is contained in a single triangle, for instance, Triangle ABC, the total number of NWs inside the triangle, N_{NW}, is ½ (three out of six slices). The total area of the wafer is the area inside the triangle, which is

$$A_W = \frac{1}{2}DH = \frac{1}{2}D^2\cos\left(\frac{\pi}{6}\right) = \frac{D^2\sqrt{3}}{4} \tag{3.8}$$

where D is the distance between SiNWs centers (as shown in Figure 12). Plugging the results of Eq. 3.8 into Eq. 3.7, we get

$$n_{NW} = \frac{2}{D^2\sqrt{3}} \Rightarrow D^2 = \frac{2}{n_{NW}\sqrt{3}} \tag{3.9}$$

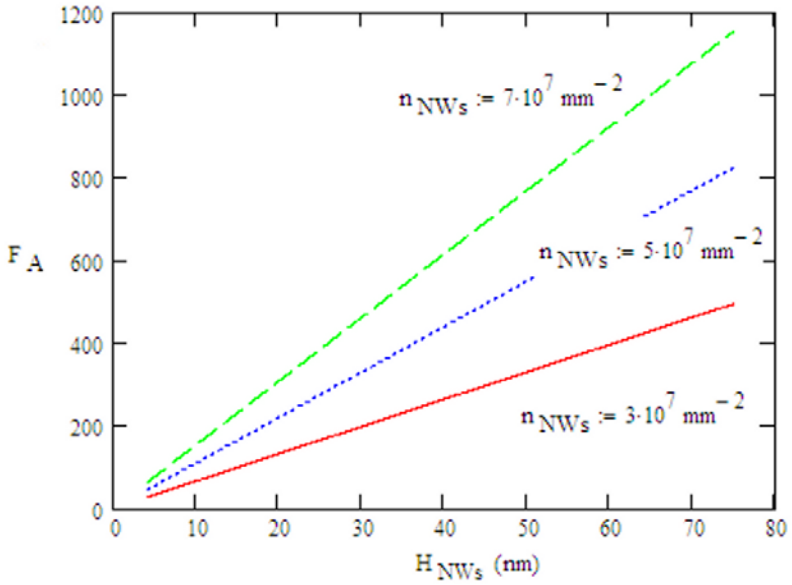

Figure 11. The area amplification factor brought about by the growth of SiNWs can be graphed according to the number of SiNWs per unit area, the height and the average width.

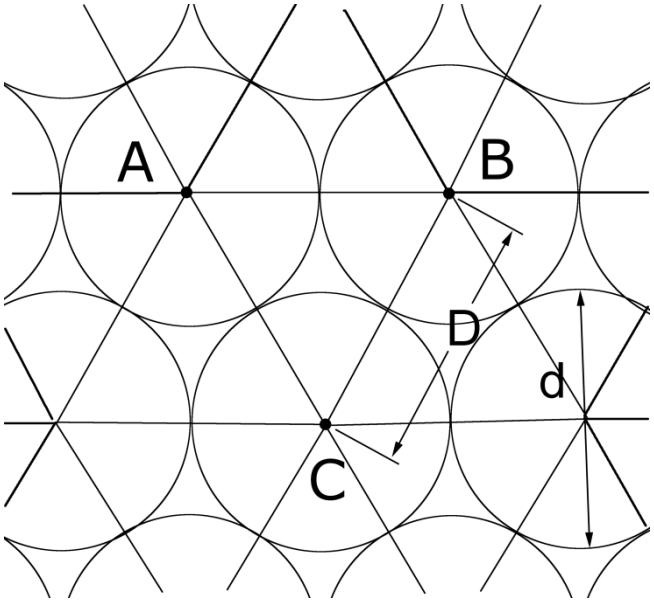

Figure 12. If the total area of a wafer is comprised of a single triangle, ABC, for instance, then the total number of SiNWs on the wafer is ½. The distance between SiNWs centers is D, while the average diameter of the SiNWs is d.

If d is the average diameter of the SiNWs (as shown in Figure 12), then d must be smaller than or equal to D and we can write

$$d_{NW}^2 \leq D^2 \tag{3.10}$$

Substituting for D^2 and noting that n_{NW} is always positive, we show that Eq. 3.6 is bound to the condition that;

$$n_{NW} d_{NW}^2 \leq \frac{2}{\sqrt{3}} \tag{3.11}$$

Oxidation of SiNWs

The oxidation of SiNWs has been done by a number of groups with a variety of goals in mind. Much of this work was done on SiNWs grown by bottom-up methods, such as VLS [78], [79] or CVD [80]. In these types of SiNWs, orientation of the SiNWs is in various directions, depending on how and in which direction the SiNWs are grown. In the special case of top down growth of SiNWs, using electroless etching, all of the SiNWs grow perpendicular to the (100) plane, so that any exposed side will always have some variation between (100) and (110) of orientation at the surface, but never any variation of (111) [78], [81], [82] The oxidation rate is higher for (110) orientations of Si than for (100) orientations, and in SiNWs, the oxidation takes place through the rotation from (100) to (110), 45° off, so that when SiNWs are oxidized, they should become "squarish," which is seen in Figures. 3a, c and e.

The first formula examined for oxide thickness was the traditional Deal-Grove model [12].

$$X_{ox} = \frac{A}{2}\left[\sqrt{1+\frac{4B}{A^2}(t+\tau)}-1\right] \tag{3.12}$$

where X_{ox} is the oxide thickness, B/A is the parabolic rate constant, B is the linear rate constant, t is the oxidation time and τ is the time for the pre-existing oxidation layer. Parabolic and linear rate constants are provided for (100) and (111) lattice orientations by Deal-Grove, but in the special case of SiNWs, these are needed for the (110) orientations.

We use the equation from Massoud, et al. [13], [14], [15] to resolve the oxide thicknesses, which are calculated from this and given in Table 4. The oxidation of SiNWs presents a special problem in this regard. The orientation of the bulk Si changes the oxidation rate, but in the case of SiNWs, the orientation is inconsistent, changing as the etching process takes place at different positions around the SiNWs. Besides this being a SiNWs problem, this is also a thin or ultrathin oxide layer problem [83], [16], [17], [18].

$$X_{ox} = \sqrt{\left(\frac{A}{2}\right)^2 + Bt + M_1\left(1 - e^{\frac{-t}{\tau_1}}\right) + M_2\left(1 - e^{\frac{-t}{\tau_2}}\right) + M_0} - \frac{A}{2} \qquad (3.13)$$

where X_{ox} is the oxide thickness, B/A is the parabolic rate constant, B is the linear rate constant, t is the oxidation time, τ_1, τ_2, M_0, M_1 and M_2 are constants defined by experimental results. Massoud, et. al., also independently developed new values in 1985 for the linear and parabolic rate constants [19]. The equations for τ_1, τ_2, M_0, M_1 and M_2 are found in Massoud, et. al. [15], along with the experimental values for the constants within.

Table 4 shows a comparison of the results for Deal-Grove and Massoud in the thin film regime, dry oxidation at 900°C, for the (100), (111) and (110) orientations and for 20, 40 and 60 minutes.

Table 4 Comparison of Deal-Grove with Massoud Thin Film Dry Oxidation

Oxidation time (min)	Oxide Thickness for (100) alignment (nm)		Oxide Thickness for (111) alignment (nm)		Oxide Thickness for (110) alignment (nm)	
	Deal-Grove	Massoud	Deal-Grove	Massoud	Deal-Grove	Massoud
20	4.5	9.4	8.8	14	8.6	15
40	8.3	15	16	22	16	22
60	12	19	23	29	22	28

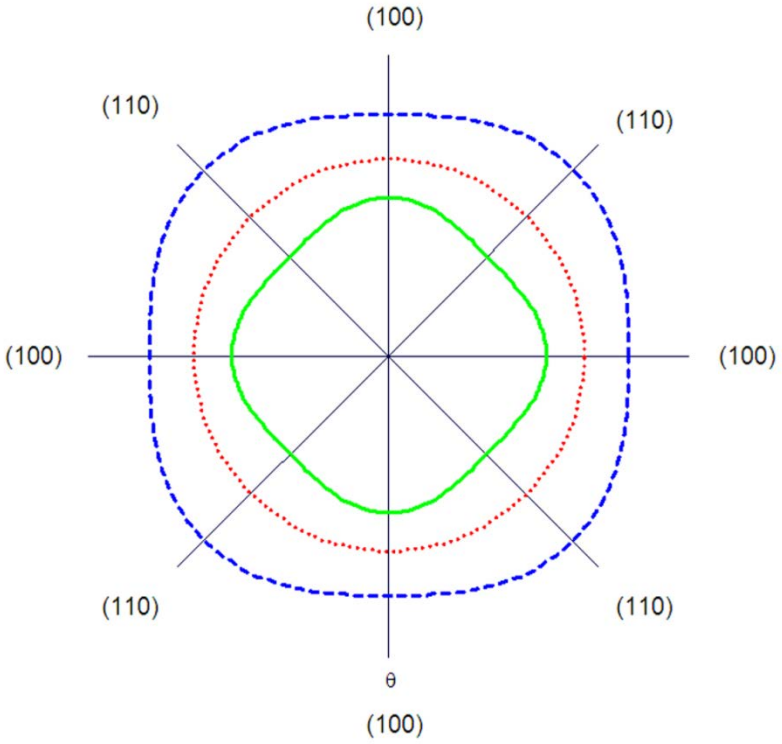

Figure 13. Graphical depiction of the oxidation of SiNWs, using a polar plot. The oxidation rate is faster for (110)-aligned Si than it is for (100)-aligned Si, which should result in uneven oxidation around the SiNW.

In order to obtain a graphic depiction of SiNWs oxidation, we can model this problem in polar form. The oxidation rate, while rotating through 2π radians of angle, changes continuously, going through eight peak alignments, beginning at the top, for example, as in

Figure 13, starts at (100), changes to (110), then to (100), then to (110) and so on. Modeling this problem with a cosine function, the peak oxidation of 100 aligned Si will occur four times around this polar plot, so the function will be cos(4θ) and the contribution at that point will be maximum, i.e. one (1). At four valleys, the peak oxidation of 100 aligned Si will be minimum (0), so the contribution at that point will be zero (0). In order to get a cosine function to provide this pattern, it must be raised by the value of one (1) and then halved, hence the formula for this function is

$$r_1'(\theta) = \frac{(\cos(4\theta)+1)}{2} \tag{3.14}$$

Modeling the other side of this problem with a similar cosine function, the peak oxidation of 110 aligned Si will occur four times around this polar plot, but off by an angle of π/4 radians, the function will be cos(4θ+π) and the contribution at that point will be "all" or one (1). At four valleys, the peak oxidation of 110 aligned Si will be minimum (0), so the contribution at that point will be zero (0). So the formula that describes this function is

$$r_1''(\theta) = \frac{(\cos(4\theta+\pi)+1)}{2} \tag{3.15}$$

The oxide thickness for (100) Si is described by Eqs. 3.12 and 3.13, and the variable that comes out of those equations is X_{ox100}. For (110) Si, a different value is obtained using the same equations, and is X_{ox110}. With these two variables defined, an equation describing the thickness of the oxide layer around a SiNW in a polar plot is written as:

$$X_{ox}(\theta) = X_{ox100}\, r_1'(\theta) + X_{ox110}\, r_1''(\theta) \tag{3.16}$$

In this equation, at the oxidation peaks, (100) and (110), the oxide thicknesses are ideally described by Eqs. 3.12 and 3.13. At all points in-between, it is assumed that a smooth transition occurs in the oxidation thickness, and there is some evidence for this [26]. While this formula approximately describes the oxidation around the SiNW using a polar coordinate system, it does not describe the shape of the SiNW subsequent to oxidation. In order to do this, the expansion ratio of Si to SiO_2 must be factored in. In these equations, it is given the variable name κ_0. In Si, the expansion ratio above the original surface is 54% or 0.54. Below the original surface, in these equations, it is described as $1 - \kappa_0$. This is the case in planar Si, but since this is a SiNW, it must be treated as a cylindrical problem. The expansion is volumetric, and so the ratio of expansion above and below the original Si surface must be related to the volumes as:

$$\frac{V_1 - V_0}{V_0 - V_2} = \frac{r_1^2 - r_0^2}{r_0^2 - r_2^2} = \frac{\kappa_0}{1 - \kappa_0} \tag{3.17}$$

where V_1 is the total volume of the oxidized SiNW, V_0 is the volume of the pre-oxidized SiNW (the volume of the original unoxidized SiNW), and V_2 is the volume of the unoxidized SiNW beneath the oxidation layer, as shown in Figure 14. The oxide layer X_{ox} from Eq. 3.16 above is related by:

$$r_1 - r_2 = X_{ox} \tag{3.18}$$

Solving for r_1 and r_2 individually and substituting each into the Eq. 3.17 above, the radii of the two layers are given by:

$$r_1 = \kappa_0 X_{ox} + \sqrt{\left(\kappa_0 X_{ox}\right)^2 - \left(\kappa_0 X_{ox}^2 - r_0^2\right)} \tag{3.19}$$

and

$$r_2 = -\left(1 - \kappa_0\right) X_{ox} + \sqrt{\left[\left(1 - \kappa_0\right) X_{ox}\right]^2 - \left[\left(1 - \kappa_0\right) X_{ox}^2 - r_0^2\right]} \tag{3.20}$$

If r_1 and r_2 are known, r_0 can be determined from:

$$r_0 = \sqrt{r_1^2 + \left(r_2^2 - r_1^2\right)\kappa_0} \tag{3.21}$$

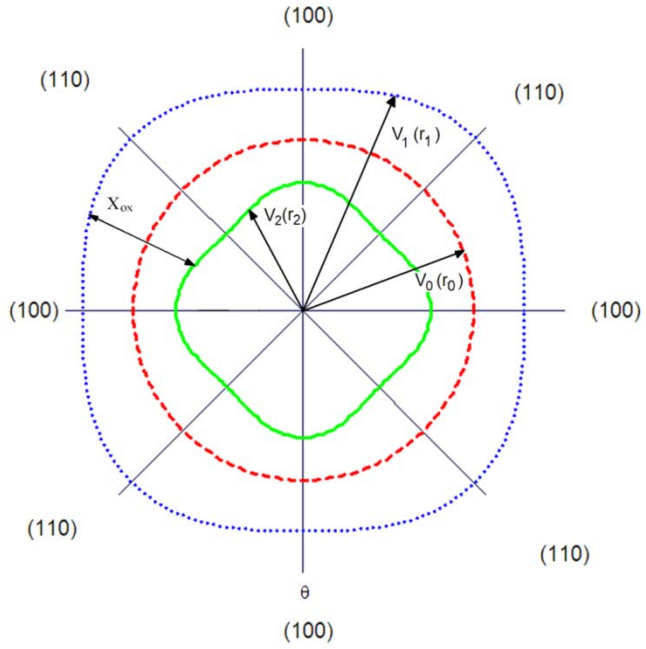

Figure 14. Volume V_1 is identified by radius r_1, V_2 by r_2 and V_3 by r_3 on an oxidized SiNW. X_{ox} is the oxide layer thickness.

For SiNWs of very large radii (relative to the oxide layer thickness), Eqs 3.19, 3.20 and 3.21 simplify to:

$$r_1 = r_0 + X_{ox}\kappa_0 \tag{3.22}$$

$$r_2 = r_0 - X_{ox}(1-\kappa_0) \tag{3.23}$$

and

$$r_0 = r_1 + \kappa_0\left(r_2 - r_1\right) \tag{3.24}$$

Results and Discussion

SEM Studies

In Figures 10a, c and e, it can be seen that the SiNWs were plainly "inflated" by having been mostly turn into SiO_2. After a standard BOE for one minute, the remaining SiNWs are shown in Figures 10b, d and f. In Figures 10d and f, there appear to be a large number of "stubs" sticking out of the bulk Si (at the bottom) which could suggest that a large number of the SiNWs were oxidized all the way through, leaving only some of the largest SiNWs behind, much thinner than they were at the start. So many stubs could also be the result of SiNWs being so thin that the force of cleaving the wafer (for examination by SEM) caused many of them to simply break off.

Sample f is in much worse condition than Sample d in this respect, and only a relative few NWs have survived (from this vantage point). Considering that the average width was around 65 nm, likely the oxide layer grown here was on the order of 70nm[3], far greater than either the Deal-Grove calculation of 12nm or the Massoud calculation of 19nm for a 60-min. dry oxidation at 900°C.

Calculations

Using the Deal-Grove and Massoud algorithms, a plot can be made that simulates the shape of the oxide layers in SiNWs by using the cosine function and plotting this in polar coordinates. When these formulas were applied to SiNWs oxidation, the results are shown in

[3] Note that the BOE for this etch was for one minute and the etch rate was 600Å/min, which would have left a 10 nm layer of oxidation behind.

Figure 15. In these figures, the dashed middle (red) line shows the original SiNWs surface (prior to oxidation), the solid inner (green) line shows the intrusion of the oxide under the original surface of the Si and the dotted outer (blue) line shows the outer surface of the oxide. The squaring effect on SiNWs is apparent in these images. This assumes that the original SiNWs shapes are perfectly round, which may not be the case.

Conclusion

It is advantageous to be able to control the size, regulation and pitch of SiNWs, which has been done by masking with silica colloidal nanoparticles [5] in large dimensioned (relatively speaking) arrays. Control of oxide thickness on SiNWs is relatively difficult and a little more complex than one might expect. Oxidizing and etching SiNWs causes them to become square-shaped because of the change of orientation around the circumference of the SiNWs. An oxide layer can be used to change the size of a set of SiNWs of all the same width, but the shape will not be "round" after oxidation and/or etching. In making SiNWs using this electroless chemical etching method, whenever (100) wafers are used, the only surfaces available for oxidation are (100) and (110), and of course, all those in-between ((120), (130), (140), and so on). No (111) surfaces are available for this type of oxidation.

We presented here a means to pictorially describe the shape of an oxidized SiNW, using a polar coordinate system and the formulas and constants supplied by previous researchers. This is a very special case where there exists a need to better understand how SiNWs are oxidized and what the implications are. For example, if SiNWs are etched in a manner such that they are too close together, too much oxidation will result in sufficient expansion as to begin breaking the SiNWs away from the substrate as they crush up against each other. Prior to this, there were no

formulas to describe this. With these formulas, we still find some discrepancy in the figures that should appear. In the one example, the time of oxidation was 20 min., but the only way to correctly suggest a reversal through the formulas was to assume an oxidation time of 110 min. So there is a definitive need to write oxidation formulas specific to SiNWs, because of their unique geometry [82].

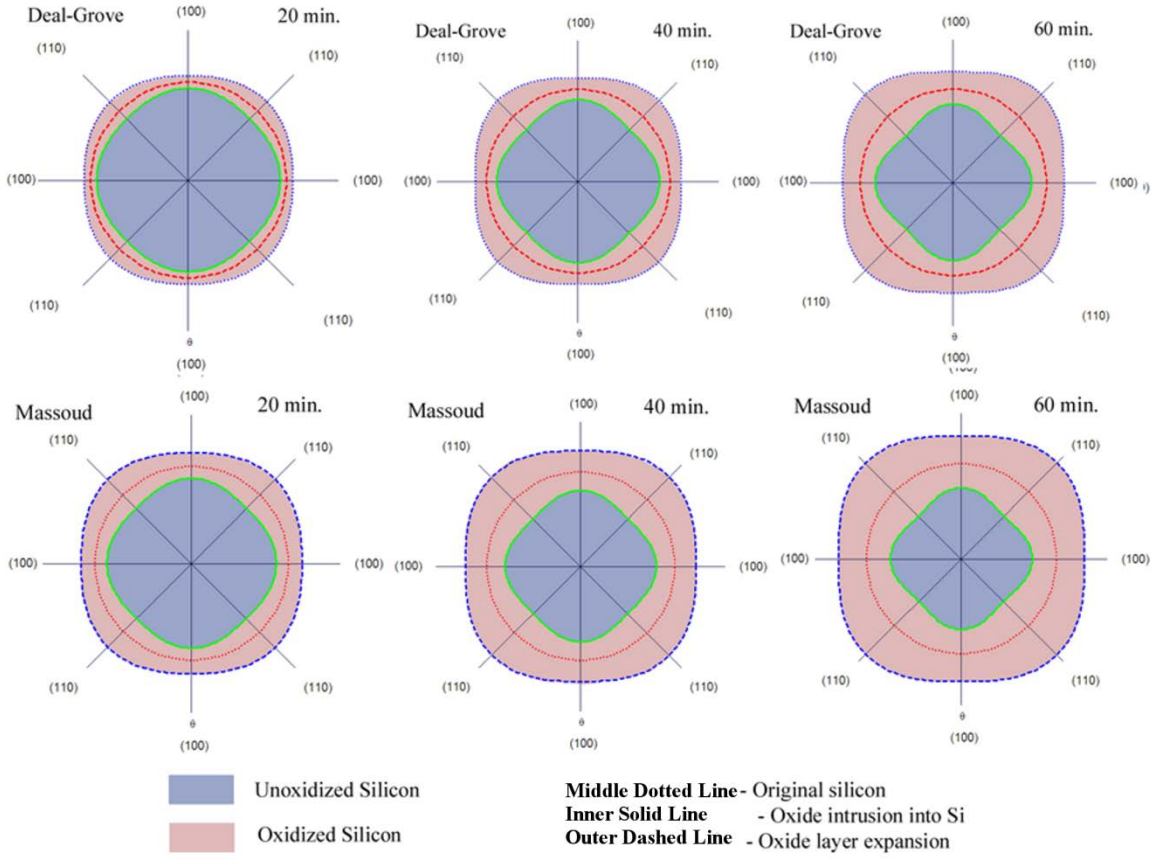

Figure 15. Comparison of Deal-Grove and Massoud oxidation equations when applied to a polar plot, simulating the dry oxidation of SiNWs at 900°C on the (100) and (110) orientations, for 20, 40 and 60 minutes.

It will be a subject of great interest to follow up on the solutions provided in the previous section. Several solutions have been offered up, mostly in the form of the heat equation, and the

freezing (or melting) of cylindrical structures. In the freezing of water, the two boundaries move, the inner as the water freezes and that boundary moves inward, and the outer as the ice expands, and that boundary moves outward. This is a relatively well-known problem and is known as a Stefan problem [27], [34].

CHAPTER 4: DIFFUSION OF DOPANTS IN SILICON NANOWIRES

Prelude

The materials presented in this chapter are part of a larger investigation of the fundamental properties of SiNWs. It is intended that the materials in this chapter will become part of a future publication. The following is a study on diffusion doping of Si with Boron and Phosphorus, fairly well understood processes for the case of planar Si, which could perhaps be improved upon, but for the greater part is mathematically complete. Having a long history, dating back to 1855 [20], [23] and basis in the science of diffusion, even cylindrical diffusion problems are somewhat well understood. Moving boundary diffusion problems are a bit more complex, as are problems with pre-existing diffusion profiles.

Diffusion doping of Si is generally a two-step process (actually, multi step, but two main steps are involved in the more complex part of diffusing dopants into Si), the first part being a pre-deposition (pre-dep) and the second part being the drive-in. The pre-dep is fairly well understood, but the drive-in, because of the use of oxidation, makes this part of the process relatively difficult to calculate. In the regular college texts, even at the graduate level, this particular subject is often avoided. Authors will usually refer to the “dose” rather than the profile, once drive-in is completed. In planar Si diffusion doping, this part of the doping process is still under investigation by some groups, so the cylindrical drive-in diffusion of dopants is only a remote consideration of most groups conducting experiments in this research area.

Of groups conducting research in the field of diffusion doping of SiNWs, most have only done research on SiNWs made by the VLS method. In general, what is observed in these

experiments and their measurements is that the doping profile is somewhat comparable to what has been predicted in this paper, although, without point-by-point analysis, this cannot be confirmed. Usually these groups have provided some mathematical function to describe the profiles they have measured, but these appear to lack the mathematical rigor and a basis in diffusion principles (Fick's Laws). No research groups are known to have conducted measurements of diffusion doping profiles in SiNWs grown by the electroless process used in these investigations.

This chapter breaks into this particular aspect of diffusion doping, and taking it further, goes into an in-depth analysis of the mathematical models of diffusion, applying these to the SiNWs. The laws of diffusion are applied to the morphology and physical conditions of the problem to arrive at a better formulation of the calculations than has been provided to date.

DIFFUSION OF DOPANTS IN SILICON NANOWIRES

Abstract

In this paper we use Fick's Laws and the properties of bulk Silicon (Si) to calculate the diffusion of dopants in Silicon nanowires (SiNWs). The morphology of SiNWs does not allow the use of the same formulas that are used in the doping and diffusion of bulk Si. While Fick's Laws still apply, the law as applied is a differential equation and different solutions must be used in order to solve this cylindrical problem.

Introduction

In recent years, Silicon nanowires (SiNWs) have become a research subject of great interest, partly because of the unique properties and partly because of their morphology.

Doping of bulk Silicon is a somewhat well-understood process these days. This is a diffusion process, which is subject to Fick's Laws and varies with temperature, relative pressures, materials, types of sources, activation energy and solid solubility limits, among other things. While research on this particular subject continues, because of the wide array of new materials and applications, another critical variable, shape, is one that has been largely ignored (however, not entirely). The shape in consideration here is that of a cylinder, which must also comply with Fick's Laws when diffusion is applied.

Literature Search

The subject of diffusion is such a large one that many books and papers were used as references in this thesis. These will be referenced as used and some will be listed as general references. The primary limitation of this search was to that of the specific diffusion of dopants into SiNWs, which is a fairly limited subject. Very few participants have taken on this work, since it is fairly difficult thing to measure, although some appear to have been somewhat successful at doing this. Their measurement methods are a subject of interest.

Koren, et. al. [36] were able to measure the doping distributions in SiNWs grown by the VLS method by using successive surface etching of single SiNWs and then measurements using Kelvin probe force microscopy (KPFM). Their results indicated an exponential decrease in doping density as the radius decreased. In this case, the NWs were doped independently of the NWs growth. This method appears to be the most promising, with reasonable accuracy and repeatability.

Perea, et. al. [37], have done measurements of doping density on gold-catalyzed Ge NWs, grown by the VLS method, using pulsed laser atom probe tomography to measure Phosphorus doping. In this case, the doping took place concurrently with the NWs growth, even so, with uneven doping distributions.

Allen, et. al. [38] (same group as above) use scanning photocurrent microsopy (SPCM), a technique involving using a focused laser to generate excess carriers, to measure the transport characteristics. This technique used SiNWs grown by gold-catalyzed VLS method. These NWs were doped during growth.

Imamura, et. al. [39] do comparative microRaman spectroscopy of single SiNWs to determine Boron concentrations on SiNWs grown by the gold-catalyzed VLS method, again, with active doping during the growth. In this case, uneven doping was also reported using this method of doping.

Garnett, et. al. [40] used capacitance-voltage (C-V) measurements to determine dopant density, however in this method, dopant density is expected to be uniform and it is assumed that the surface charge is known. The measurements were made on nanowire field-effect transistors (FETs) grown epitaxially using the gold-catalyzed VLS method. The doping was conducted separately through diffusion with a Boron source. They were able to obtain a experimental radial doping profiles using these methods with only minor deviations from the simulations.

Fick's Laws

Fick's first law of diffusion states that the flux (J) is proportional to the negative of the concentration gradient ($\partial C/\partial x$). The flux, in this case, is the movement of particles through a material, but this is also used in heat transfer, so can represent the movement of heat through a material. In this formula, D is the diffusion coefficient, C is the doping concentration and x is the depth into the substrate.

$$J = -D\frac{\partial C}{\partial x} \tag{4.1}$$

Fick's second law states that

$$\frac{\partial C}{\partial t} = -\nabla J \tag{4.2}$$

where t is the time. Combining Equations (4.1) and (4.2) gives us the form

$$\frac{\partial C}{\partial t} = D\nabla^2 C \tag{4.3}$$

This can also be written in the form

$$\frac{\partial C}{\partial t} = D\frac{\partial^2 C}{\partial x^2} \tag{4.4}$$

This is the general form of the equation, although if the problem comes in cylindrical form, the depth, x, is replaced with the radial depth, r, the cylindrical form of this equation is

$$\frac{\partial C(r,t)}{\partial t} = D\frac{1}{r}\frac{\partial}{\partial r}r\frac{\partial C(r,t)}{\partial r} \tag{4.5}$$

The boundary conditions of this problem vary according to a number of factors, including the type of material (Boron or Phosphorus) and the stage of diffusion (pre-deposition or drive-in). In the general case there are some basic conditions to start with:

For $r = R$ and $t \geq 0$, $C = C_0$,

For $0 < r < R$ and $t = 0$, $C = f(r)$.

This problem is often solved by separation of variables, assuming that the two variables in this equation are linearly independent, but have the one case of both sides having an equal constant, as

$$C(r,t) = R(r)\cdot T(t) \tag{4.6}$$

$$\frac{1}{R\cdot r}\frac{\partial R}{\partial r} + \frac{1}{R}\frac{\partial^2 R}{\partial r^2} = -\lambda^2 \tag{4.7}$$

and

$$\frac{1}{T}\frac{\partial T}{\partial t} = -\lambda^2 D \tag{4.8}$$

The solution to Eq. (4.8) is

$$T = Ae^{-\lambda^2 Dt} \tag{4.9}$$

Eq. (4.7) can be rewritten as

$$r^2R''+rR'+r^2\lambda^2R = 0 \tag{4.10}$$

There are variations on this equation, depending on the boundary, initial and final conditions, but this is Bessel's equation. The solution to this equation, in its general form is

$$R = BJ_0(r\cdot\lambda) + CY_0(r\cdot\lambda) \tag{4.11}$$

where J_0 is a Bessel function of the first kind and order zero and Y_0 is a Bessel function of the second kind and zero order. Since $Y_0 \rightarrow \infty$ as $r \rightarrow 0$, C = 0, in order to avoid a singularity, so that Eq. (4.11) reduces to

$$R = BJ_0(r\cdot\lambda) \tag{4.12}$$

Another singularity that must be avoided is a discontinuity across the outer boundary. That is to say that, at the boundary, $r = R_0$, $C = C_0$ for all t's ($0 < t < \infty$). This condition will be met for all cases of the solution of R such that

$$J_0(R_0\cdot\lambda) = 0 \tag{4.13}$$

This condition occurs at the positive roots of J_0, so that this equation can be rewritten as

$$J_0\left(\frac{\alpha\cdot r}{R_0}\right) = 0 \tag{4.14}$$

where

$$\lambda = \frac{\alpha}{R_0} \tag{4.15}$$

where α is a positive root of $J_0(x) = 0$.

Combining Eqs. (4.9) and (4.12) with Eq. 4.14, and making the appropriate substitutions, we get

$$C(r,t) = Ae^{-\frac{\alpha^2}{R_0^2}Dt} J_0\left(\frac{\alpha \cdot r}{R_0}\right) \tag{4.16}$$

This equation is true for all positive roots of Eq. (4.14), so that it can be expanded in a summation to include all positive roots of this equation in the form

$$C(r,t) = \sum_{n=1}^{\infty} Ae^{-\frac{\alpha_n^2}{R_0^2}Dt} J_0\left(\frac{\alpha_n \cdot r}{R_0}\right) \tag{4.17}$$

Variations on this solution will depend on other boundary and initial conditions as they arise, which will provide solutions when solving for A.

In the special case of oxidation diffusion, there is another boundary at the Si/SiO_2 interface during the drive-in, at which the same boundary conditions must be met. That is to say that, on either side of the Si/SiO_2 boundary, the concentrations of dopants must be the same. This can be taken to one more level, subsequent to the oxide removal, to say that, when the concentration at the outside of the surface is zero (0) after the oxide layer is removed, the concentration just inside the Si surface must also be zero.

Diffusion

There are other boundary conditions relating to the two-part diffusion process. The first part of the diffusion process is the pre-deposition (pre-dep), wherein an initial layer of dopant is diffused into the substrate, in this case, Si. The surface concentration is taken to be constant and to be in infinite supply.

The solution to this problem is a two-part combination of zeroth order Bessel functions of the first kind (see Appendix C for a brief description of Bessel functions and for a brief description of the Gamma function). For the first step of a two-step diffusion, we take the initial concentration, f(r) to be zero [27], [34], [24], [25]. Using Eq. (4.7) and solving, we get

$$C = C_0\left[1-\frac{2}{R}\sum_{n=0}^{\infty}\frac{1}{\alpha_n}\frac{J_0(r\cdot\alpha_n)}{J_1(R\cdot\alpha_n)}\cdot e^{-D\cdot\alpha_n^2\cdot t}\right] + \frac{2}{R^2}\sum_{n=0}^{\infty}\frac{J_0(r\cdot\alpha_n)}{J_1^2(R\cdot\alpha_n)}\cdot e^{-D\cdot\alpha_n^2\cdot t}\cdot\left(\int_{r=0}^{R} r\cdot f(r)J_0(r\cdot\alpha_n)dr\right) \quad (4.18)$$

When f(r) is zero, the second term of Eq. (4.9) goes away, and the initial pre-dep is the result of only the first term. We establish some of the variables and formulas used in this calculation:

E_A = 3.69 eV – activation energy (same for Phosphorus and Boron) [20]

D_0 = 10.5 cm^2/sec – diffusivity (same for Phosphorus and Boron) [20]

N_{B0} = 1.1 x $10^{20}/cm^3$ – surface concentration for Boron during pre-dep [20]

N_{P0} = 3.8 x $10^{20}/cm^3$ - surface concentration for Phosphorus during pre-dep [20]

C_0 = $0/cm^3$ – surface concentration during drive-in using Eq. (5.9)

C_0 = N_{B0} or N_{P0} during pre-dep. This is the surface concentration

k_B = 8.617 x 10^{-5} eV/K – Boltzman constant

T = 1098.15K – temperature in Kelvin (825°C)

R = 50 nm – The initial radius of the SiNW in this simulation

α_n's are the positive roots of $J_0(R\alpha_n)$ = 0 (11 roots are listed in Table 5 in Appendix C)

A comparatively low temperature was selected for this model because of the smallness of SiNWs and the problem at hand. SiNWs are very small, and the traditional temperatures could be selected for these processes, but the diffusion times, in order to get the very small doping profiles, would be impracticably short (25s, for example, would not be achievable in a standard diffusion oven).

The diffusion coefficient is temperature-dependent, which is expressed by the formula

$$D = D_0 e^{-\left(\frac{E_A}{k_B T}\right)} \tag{4.19}$$

For bulk Si, using Boron, the solution to Eq. (4.4) [21] is the doping profile after pre-dep, N_b, subscripted "b" to denote a "bulk" profile.

$$N_b = N_{B0}\,\mathrm{erfc}\left[\frac{(R-r)}{2\sqrt{Dt}}\right] \tag{4.20}$$

For cylindrical SiNWs, using Boron, the solution to Eq. (4.5) [27], [34], [24], [25] is the doping profile after pre-dep, N_c, subscripted "c" to denote a "cylindrical" profile.

$$N_c = N_{B0}\left[1 - \frac{2}{R}\sum_{n=0}^{\infty}\frac{1}{\alpha_n}\frac{J_0(r\cdot\alpha_n)}{J_1(R\cdot\alpha_n)}\cdot e^{-D\cdot\alpha_n^2\cdot t}\right] \tag{4.21}$$

This is the first term of the solution of Eq. (4.18), where the second term is zero, by assuming that there is no doping prior to pre-dep. In general, this is never the case, since this would suggest the substrate is intrinsic material. The more general case is that the doping ahead of a pre-dep is of the opposite material type. In another case, there could also be an existing doping level which would be constant throughout the substrate material. A comparison of these two solutions is shown in the graph of Figure 16.

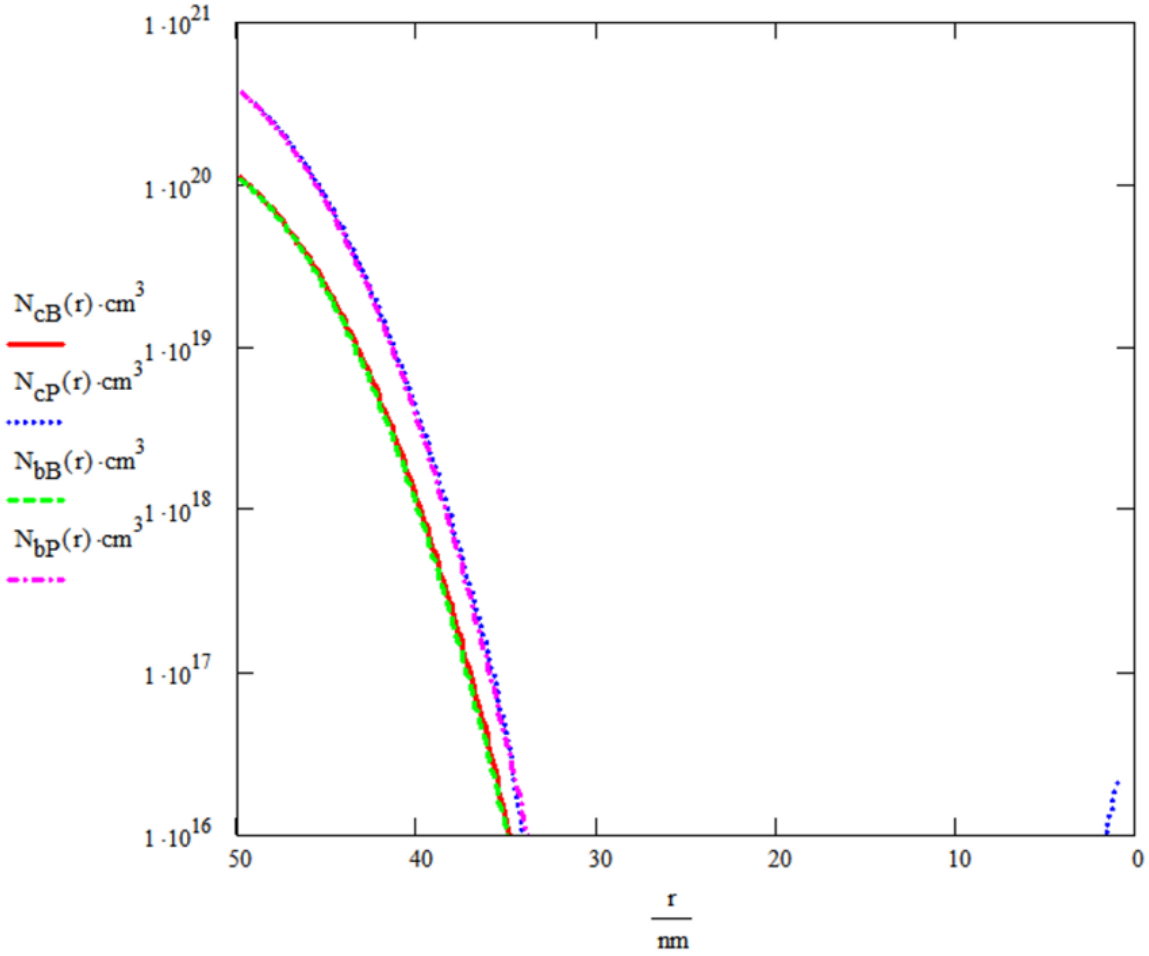

Figure 16. Pre-dep doping profiles N_{cB} (cylindrical Boron), N_{cP} (cylindrical Phosphorus), N_{bB}(planar Boron), and N_{bP} (planar Phosphorus) using Eqs. (5.11) and (5.12) modeled in Mathcad.

During the pre-dep, the chemical reaction is the result of the Boron or Phosphorus material used. Some common materials used for this reaction are B_2O_3 (Boron trioxide/Boron oxide/Diboron trioxide) and P_2O_5 (Phosphorus pentoxide). The chemical reactions are

$$2B_2O_3 + 3Si \rightarrow 4B + 3SiO_2 \tag{4.22}$$

$$2P_2O_5 + 5Si \rightarrow 4P + 5SiO_2 \tag{4.23}$$

Post Boron pre-dep procedures include a Borosilicate etch, which begins with a buffered oxide etch (BOE) to remove existing SiO_2, followed by a dip in H_2SO_4:HNO_3 to oxidize the remaining Boron components, and then another BOE to remove that oxide layer. Post Phosphorus pre-dep procedures may or may not involve a deglazing step, to remove Phosphosilicate. In general, after the pre-dep, the surface is considered to no longer be a source for dopants. A drive-in diffusion is usually done by oxidation, at which point, the segregation and transport coefficients must be taken into account.

Drive-In

Once a doping profile has been established inside the substrate, the subsequent profile, when done by oxidation, will depend heavily upon what type of dopant is being driven. When Phosphorus is being driven, any dopant at the edge of the SiO_2/Si interface during the drive-in will "pile-up" on the Si side of the interface. In this case, the SiO_2 acts as a barrier, to some degree, to diffusion, which disallows diffusion into the SiO_2 and forces the existing dose to be used more efficiently. In the case of Phosphorus, the segregation coefficient is very high – on the order of 2500. The mathematics of this interface presents it as a very nearly solid barrier to diffusion. There is some simplification of this problem in knowing this, but some complication in the fact that it is a moving boundary.

When Boron is being driven, the segregation coefficient is less than 1, so at the SiO_2/Si interface, a great deal of the dopant leaches into the SiO_2 from the Si and is lost. Dopant material close to the surface will escape, so the oxide layer is not a good barrier to loss. At the interface, the profile of the dopant on the Si side looks like a "pile-down." This is also a moving boundary, which complicates the mathematical problem.

Subsequent to the drive-in, the oxide layer is removed, taking with it, any dopants that have leached into it. In the case of Boron, it will be heavily laden with dopants. In the case of Phosphorus, very little dopant material will have been lost. The end result of this is that each of these cases must be treated differently, mathematically. Because we are comparing nanoscale devices, we expect very shallow oxide layers, using substantially lower temperatures and shorter diffusion, oxidation and etching times. In a general doping profile, one might expect to end with a doping profile with a depth of up to several microns. In this case, the doping profile depth should be no more than 20 nm.

In order to solve these problems, it must be assumed that groups of dopant atoms can be treated separately, even if they are in the same group to begin with. This is to say that, barring interactions between dopant atoms, such as bumping into each other or creating an electrical field gradient that causes like dopant atoms to separate for instance, we can assume that two equal groups of dopant atoms, occupying the same substrate, can be treated with separate equations, knowing in advance that the atoms in these two groups have different destinations. This might be suggested as a principle of non-interaction between dopant atoms. Boron and Phosphorus drive-ins must be treated very differently.

Cylindrical Boron Drive-In

With an existing Boron profile deep within the substrate, whether it is a NW or a planar surface, the oxide layer acts like a sponge, soaking up and rapidly diffusing any dopant atoms that get near the Si/SiO_2 interface. The segregation coefficient at this interface is m = 0.43 [84]. This means that the doping density inside the SiO_2 layer is 2.33 (1/0.43) times higher than the doping density just inside the SiO_2 layer. This amounts to a “pile-down” at the Si/SiO_2 interface.

To calculate this is a three-step process, beginning by treating all of the dopant atoms in the pre-dep profile first as being inside a "leaky" surface, wherein all dopant atoms that diffuse near the outer surface are dissipated away from it and lost.

This will be even more the case if the substrate is the SiO_2, which diffuses Boron much more rapidly than does Si. However, we exclude this in the initial part of our calculation and ignore the SiO_2 completely. The formula that best describes this process is Eq. (4.18) above, except that now we use only the second part, since there is no surface supply of doping material.

$$C(r) = \frac{2}{R^2} \sum_{n=0}^{\infty} \frac{J_0(r \cdot \alpha_n)}{J_1^2(R \cdot \alpha_n)} \cdot e^{-D \cdot \alpha_n^2 \cdot t} \cdot \left(\int_{r=0}^{R} r \cdot f(r) J_0(r \cdot \alpha_n) dr \right) \quad (4.24)$$

In this equation, f(r) is the initial doping profile, which was provided by the pre-dep equation (5.12). The result of this calculation is shown in Figure 17 with some variables provided as follows:

t = 600s - diffusion and drive-in time for all examples.

T = 825°C – this is the diffusion and (single, wet) drive-in temperature for all examples.

$N\alpha = 15$ – the number of Bessel zeros used in the calculation.

$N\beta = 250$ – number of Fourier series n's.

R = 50 nm – the outer beginning radii of the SiNWs.

r_{2B} = 48.585 nm – the calculated radius of the intrusion of the oxide layer into the SiNW, using the formulas from [66] for <100> aligned Si.

In Figure 17, the cylindrical doping drive-in profile is shown as the dot-dash (pink) line on this logarithmic graph. Note that it differs from the other profiles in that it dips near the

surface (r = 50 nm), the result of the equation that generated this curve, indicative of the fact that, near the surface, dopant dissipates away and is lost. In reality, all of these curves should show their curves dipping to zero near the edge, except for the existence of the SiO_2 layer, which is not shown here. With or without the SiO_2 layer, the planar Boron sample also exhibits this quality.

Planar Boron Drive-In

The planar Boron drive-in profile is guided by

$$C(t,r) = \frac{S}{\sqrt{\pi Dt}} e^{-\left(\frac{R-r}{2\sqrt{Dt}}\right)^2} \operatorname{erf}\left(\frac{R-r}{2\sqrt{Dt}}\right) \tag{4.25}$$

where S is the dose per square centimeter. The dose is determined by calculating the area under the curve of N(r,t), where N(r,t) is the pre-dep profile given in Eq. (4.20). The pre-dep profile for planar Si is defined as a complimentary error function (erfc), and based on the surface concentration N_0, also called the *solid solubility limit*. During the drive-in, Boron leaches out of the substrate, either through the surface or through the growing oxide layer. This leaching is shown as the error function attached to Eq. (4.25). The dose for planar Si is calculated as

$$S = \int_0^R N(r,t)dr \tag{4.26}$$

The results of Eq. (4.25) are shown in Figure 17 as the solid (red) curve labeled C_{bB}. In this curve and the one for cylindrical SiNWs, we see the similarities as a result of consumption of Boron near the surface. More importantly, what can be observed here, shown from the equations, is the main difference between a planar diffusion and a cylindrical diffusion. While

the surface concentrations must be the same (both are zero in this case, but reach similar peaks inside the substrate) the internal profile shows a compression of the cylindrical profile that is not apparent in the planar profile, which is the result of increased doping concentration as the inner core is approached. A calculation of the doses for equivalent diffusions, in Figure 18, shows that these two contain about the same number of dopant atoms.

Cylindrical Phosphorus Drive-In

With an existing Phosphorus profile deep within the substrate, whether it is a NW or a planar surface, the oxide layer acts like a moving wall, pushing any dopant atoms near the Si/SiO_2 interface back into the Si. The segregation coefficient at this interface is m = 2650 [84]. This means that the doping density inside the SiO_2 layer is almost zero, relative to the doping density in the Si. This amounts to a "pile-up" at the Si/SiO_2 interface. To calculate this is a three-step process, beginning by treating all of the dopant atoms in the pre-dep profile first as being inside a solid, inescapable wall, wherein all dopant atoms are retained and none are lost. We grant that a small number, one in 2650, are lost, either to the SiO_2 or to the outer surface, but that number is fairly small. For a cylindrical profile, the equation guiding the pre-dep is the same as for the Boron. However, for the drive-in, Boron was prone to escape, whereas Phosphorus most nearly cannot. This is taken to be a cylinder with an existing profile, $f_{cB}(r)$, and no flux across the outer surface. It is assumed, for the sake of simplicity, that as soon as the oxide layer starts to form, which is right away, no Phosphorus crosses the outer layer. The equation satisfying this condition [25] is

$$C_{cP}(r,t) = \frac{2}{R^2}\int_0^R r \cdot f_{cP}(r,t) \cdot dr + \frac{2}{R^2}\sum_{n=1}^{N\alpha} e^{-D\alpha_n^2 \frac{t}{R^2}} \frac{J_0\left(\frac{r\alpha_n}{R}\right)}{J_0^2(\alpha_n)} \int_0^R r f_{cP}(r,t) J_0\left(\frac{r\alpha_n}{R}\right) dr \tag{4.27}$$

where α_n are the roots of $J_1(\alpha) = 0$. The result of this equation is shown in Figure 17, as the dotted (green) curve. In real life there cannot be a singularity at the surface, which is a problem with the representation. However, the oxide layer is also not shown in this figure, so we have yet to deal with that.

Planar Phosphorus Drive-In

The planar Phosphorus drive-in profile is guided by an equation very similar to the one for Boron, except without the error function correction for loss of dopant;

$$C_{bP}(t,r) = \frac{S}{\sqrt{\pi Dt}} e^{-\left(\frac{R-r}{2\sqrt{Dt}}\right)^2} \tag{4.28}$$

where S is the dose per square centimeter. The dose is given by Eq. (4.26). In a manner similar to the drive-in for cylindrical Phosphorus, the oxide layer pushes back the dopant atoms as it grows inward, so it acts like a wall, blocking off any diffusing atoms, and pushing back any attempt to cross the Si/SiO_2 interface. The segregation coefficient is m = 2650, which is close enough to call "zero" for our needs here and now. Eq. (4.28) does this nicely, however, once again with a singularity at the surface of the substrate. The result of this equation is shown in Figure 17, as the dotted (blue) curve.

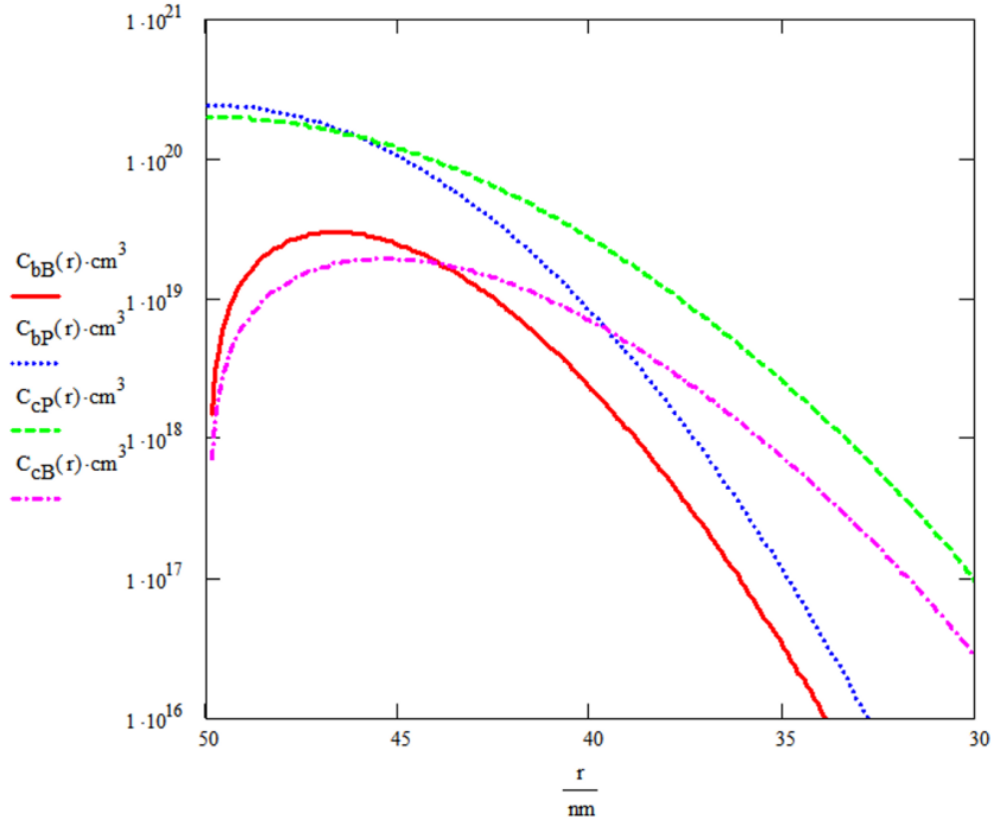

Figure 17. Drive-in doping profiles for C_{cB} (cylindrical Boron), C_{bB} (planar Boron), C_{cP} (cylindrical Phosphorus), and C_{bP} (planar Phosphorus).

Again, there is an oxide layer to contend with, and a singularity can be dealt with in the removal of the oxide layer. A comparison of the two Phosphorus curves, planar and cylindrical, reveals a situation similar to a comparison of the curves for Boron, with the exception of the drop-off at the surface. A comparison of the doses, in Figure 18, shows that both curves have about the same impurity dose, but the cylindrical curve goes more deeply into the substrate because of the increased doping density due to compression of the diffusion as it moves towards the center (r = 0 nm).

$$Q_{bB}(r) := \int_0^R \int_0^{2\pi R} \int_0^{100nm} N_{bB}(r)\, dx\, dy\, dr \qquad Q_{bB}(10nm) = 1.054 \times 10^4$$

$$Q_{cB}(r) := \int_0^R \int_0^{2\pi} \int_0^{100nm} N_{cB}(r)\, r\, dz\, d\theta\, dr \qquad Q_{cB}(10nm) = 1.029 \times 10^4$$

$$Q_{bP}(r) := \int_0^R \int_0^{2\pi R} \int_0^{100nm} N_{bP}(r)\, dx\, dy\, dr \qquad Q_{bP}(10nm) = 3.643 \times 10^4$$

$$Q_{cP}(r) := \int_0^R \int_0^{2\pi} \int_0^{100nm} N_{cP}(r)\, r\, dz\, d\theta\, dr \qquad Q_{cP}(10nm) = 3.554 \times 10^4$$

Figure 18. Calculations of the doses four curves shown in previous figures, assuming equal areas for each diffusion.

Fourier Series Modification to the Profiles

Until now the oxide layer and the singularity problems have been ignored, in the interest of getting general solutions to these diffusion problems. A Fourier series can be used to model a non-shear drop-off of the doping density in the interface between two media, such as Si/SiO_2. A good example of this non-shear drop-off can be seen in [84] in the SIMS measurement of both the Arsenic and the Phosphorus doping profiles. A Fourier series can also be modulated, by the number of iterations, to simulate the rate of the drop-off. The formula for a Fourier series square wave function is shown in Appendix C. An example of how a Fourier series can be modified to this application is given as

$$S_N(r) = \frac{1}{2} + \frac{2}{\pi} \sum_{n=1}^{N\beta} \frac{\sin\left[(2n-1)\left[\frac{\pi\left(r + R - r_2 + \frac{\psi R}{N\beta}\right)}{R}\right]\right]}{(2n-1)} \tag{5.19}$$

where Nβ is the number of iterations in the series, R is the radius of the NW or the depth of the planar diffusion, r_2 is the lower depth of the oxide layer intrusion into the original Si surface, also the location beneath the surface of the Si/SiO_2 interface, referenced from the center of the NW and ψ is the shift ratio adjustment. In this equation, the width of the "square wave" generated by the Fourier series is 2R, so there is no more than one level shift in the region of zero to R. Selection of the point of the level shift is in the numerator above the R denominator. While the term, $r + R - r_2$ selects the point precisely at the Si/SiO_2 interface, this places the center of the shift, where SN = ½, right at the interface, which would be an incorrect representation of a non-vertical rise in dopant level. An additional term, directly related to the periodicity and the number of iterations, R/4Nβ, is added to shift the point slightly to the right, causing the Fourier series to intersect with the Si/SiO_2 interface at the bottom of the curve, rather than the center. This is better described in Figure 19, which shows the Fourier equations, without and with the shift, and the resulting graph of these two functions. In this figure, the Si/SiO2 interface is represented with a Heaviside (step) function.

The end result of this is to create a non-singular shift in doping density at the Si/SiO_2 interface, which is depicted in this illustration as the squared-up curve (created using a Heaviside function). The rate of this shift can be modulated with the number of iterations, Nβ.

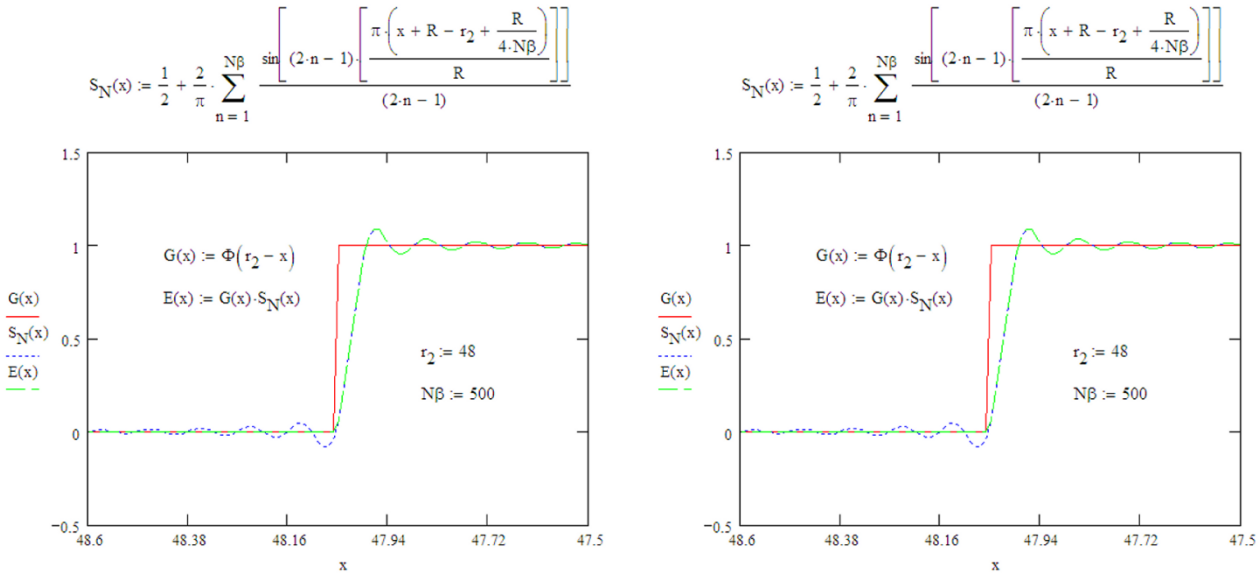

Figure 19 Fourier series square wave generator without (left) and with (right) a shift to the right to move the center.

Heaviside Function Modification of the Profiles

The introduction of Figure 19 into this discussion brings up the question of how to clean up the harmonics in the Fourier series. On the oxide side, a Heaviside, or step, function can be used to essentially zero-out any Fourier series harmonics. These act as amplifiers in the oxide, where it is well understood that no dopant will remain after the oxide layer is removed. Multiplying these two well-aligned functions will eliminate harmonics in the oxide layer and serve to define the Si/SiO_2 interface. On the Si side of the Si/SiO_2 interface, the Fourier series will modify the doping profile with a set of harmonics that are undesirable. With an Nβ value of 100, the Fourier harmonics are fairly exaggerated, as shown in Figure 20.

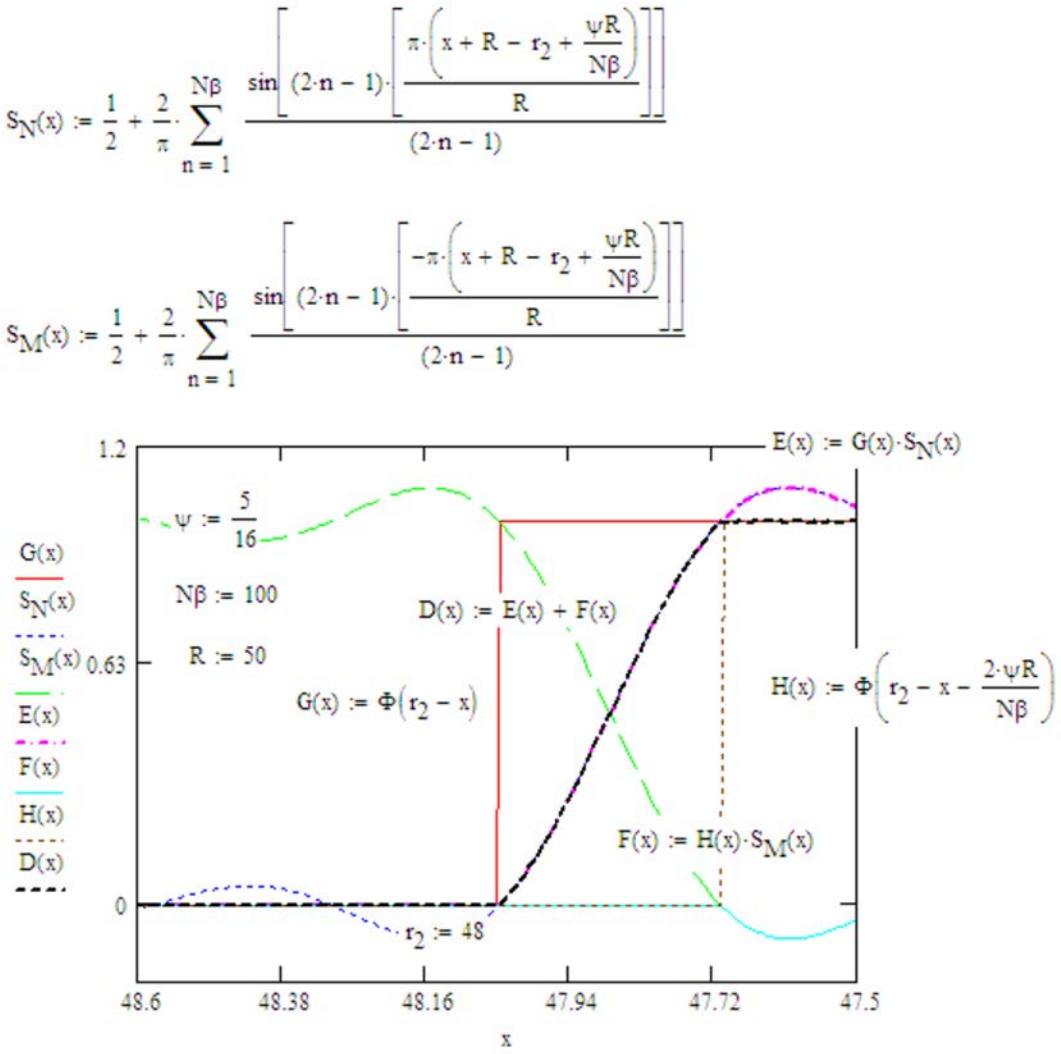

Figure 20. A combination of two Fourier series and two Heaviside functions work to form a modifying function to show a dopant distribution (not shown here).

On the left, the harmonics are neutralized with a Heaviside function, centered at the Si/SiO_2 interface. Two Fourier series are shifted to the right, but opposite values. The first Fourier series, SN(x), is modified by the Heaviside function, G(x), which becomes E(x), while the second Fourier series SM(x), is modified by a second Heaviside function, H(x), which has been shifted by twice the value of the Fourier series, becoming F(x). Adding the two functions

becomes D(x), which is shown in Figure 20 as a combination of the two Heaviside functions and the two Fourier series. On the right side, the Fourier series effectively cancel each other out.

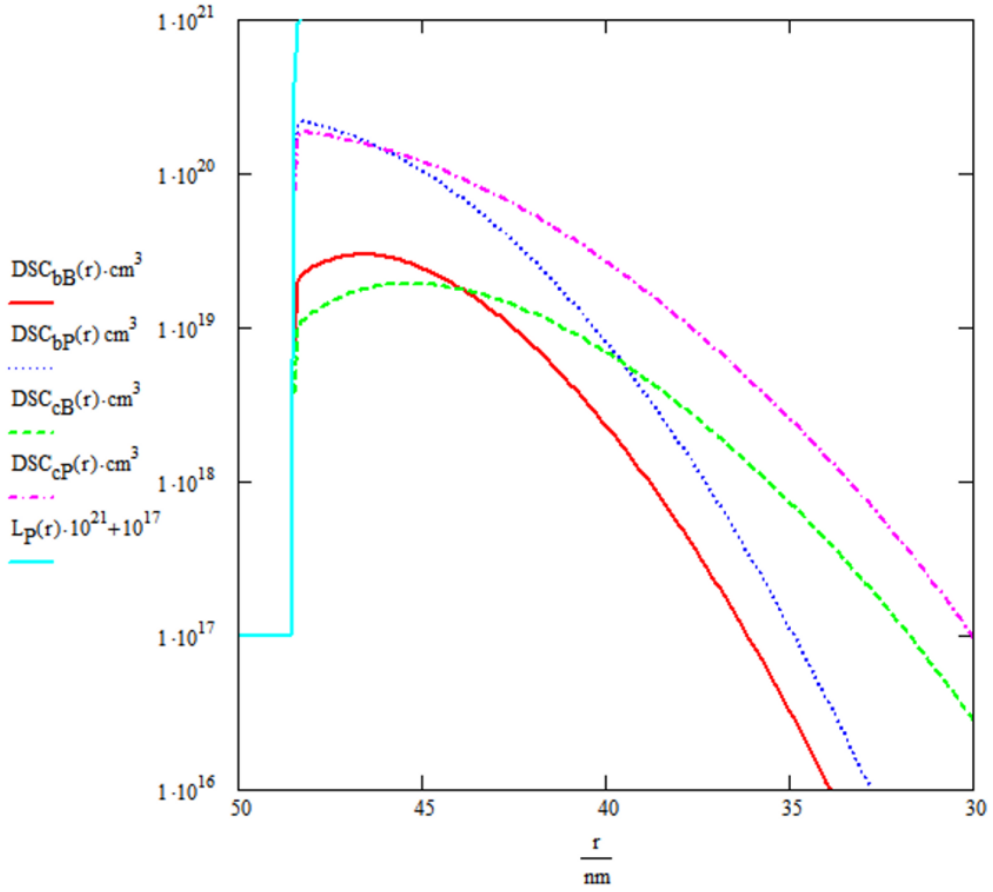

Figure 21. Post oxidation etch leaves behind the Si depth profile after application of the Heaviside functions and Fourier series modifying functions. Shown here are the planar Boron (DSC_{bB}), planar Phosphorus (DSC_{bP}), cylindrical Boron (DSC_{cB}) and cylindrical Phosphorus (DSC_{cP}).

Oxidation Removal and Post Etching

During etching, or removal of the oxidation layer that was created as a part of the drive-in process, some part of the dopant was removed, and depending on which type of dopant was used, it will be a little or a lot. With Boron, much of the dopant is removed with the oxide layer which,

during oxidation, has absorbed much of the Boron through diffusion, on account of Boron having a much higher diffusivity in SiO_2 than in Si. With Phosphorus, most of the dopant was pushed into the Si. These take place whether the morphology is planar or cylindrical. Application of the Heaviside and Fourier series to the curves in previous figures results in the curves of Figure 21, which represents the curves after the oxide layer has been removed. The thickness and intrusion of the oxide layer was calculated according the equations of Massoud [13], [14], [15]and applied using the equation developed by Mertens, et. al in [66].

Pile-up and Pile-down of Diffusants

Up to this point, most everything has been covered, providing a new calculation of dopants in SiNWs, and a comparison to the planar diffusions. What has not been discussed is one thing that changes the doping profile almost entirely, especially for Boron. As mentioned in previous sections, during the drive-in, Boron is essentially depleted from the pre-dep because of the oxide layer that consumes it.

Conclusion

It seems a bit contradictory that, in the very first diffusion, both the planar and cylindrical profiles looked very nearly identical, except perhaps for a slight difference in the profiles between Boron and Phosphorus, as shown in Figure 16. Subsequent figures show quite a bit of difference in the profiles after the drive-in. However, a comparison of the actual diffusion numbers, line-by-line, or nm-by-nm, shows a subtle difference in the two sets of curves. These two curves, using the same diffusion times and temperatures, but two completely different equations, look very nearly identical. Figure 22 shows the ratio of the planar profiles to the

cylindrical profiles for Boron and Phosphorus, and as we can see, the ratios deepen as the curves move more deeply into the substrate. At the surface, the profiles are identical, being in compliance with their respective boundary conditions (which should be the same for all cases). We can also see that the ratios are identical for both the Boron and the Phosphorus, so it is only the curves that make this difference. What we also observe is that this curve is *linear*, up to a point (beyond with these curves are relatively undefined).

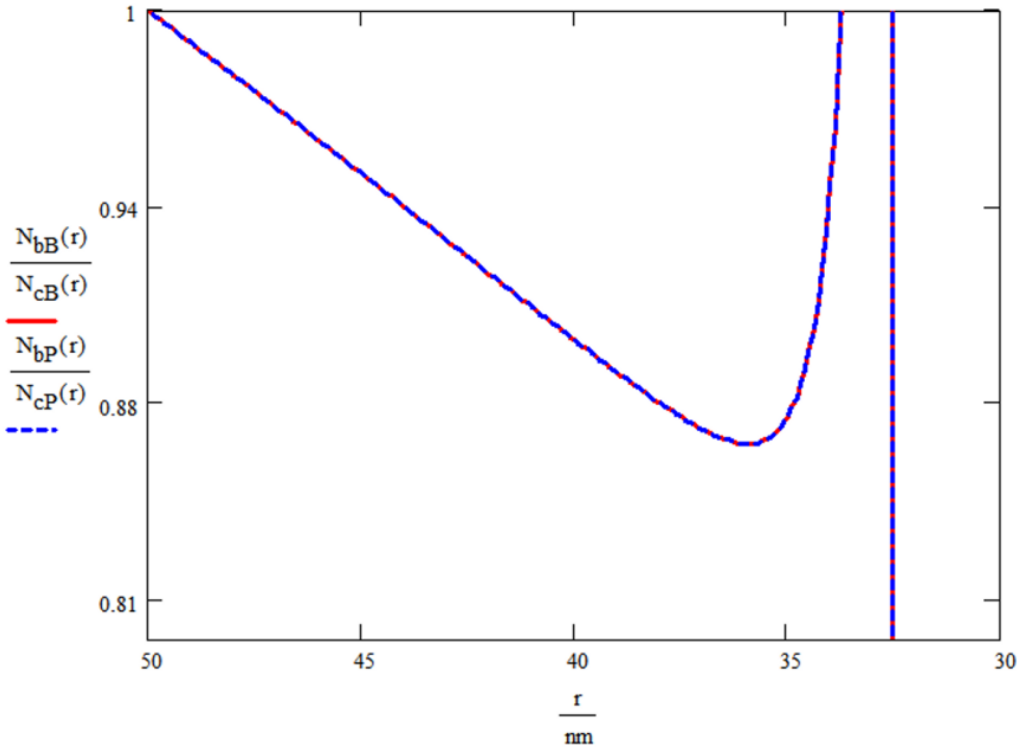

Figure 22. Ratio of planar profile (sub-b) to cylindrical profile (sub-c) for Boron (sub-B) and Phosphorus (sub-P) (only two curves are here, this is the division of N_b/N_c).

There being a linear relationship between these curves, we can write a formula to relate them. However a change in the diffusion temperature changes this curve, as does the excitation energy and the diffusion time, so any curve defined by this set of values will be short-lived

without some more definition. A change in the surface concentration will not change the curve, since both formulas begin with these as coefficients.

A better description of the pile-up and pile-down of diffusants would be desirable, but in the current thesis, time prohibits this excursion. This will certainly be pursued in future exercises. Part of the problem in this area is that, during the drive-in, the calculation must include a moving boundary, which makes it a Stefan problem. There are many solutions to this, but some shortcuts will likely have to be taken. Just the oxidation, by itself, is a moving boundary diffusion problem, having nothing to do with the diffusion of dopants.

CHAPTER 5: CONCLUSION

Oxidation

Many questions remain about SiNWs, which beg to be investigated. Among these questions and problems are oxidation and agglomeration. While the oxidation problem was addressed in Chapter 3 of this thesis, this only addressed part of the problem. The oxidation formulas developed by previous scientists only worked for planar Si, while these formulas were developed specifically for cylindrical morphology, while ignoring the plain and obvious fact that the oxide layer thicknesses were wrong for this morphology. It was good to see that the oxidation growth pattern would be "squarish," looking at oxidized SiNWs from the top. This problem can be approached as a moving boundary problem, also called a "Stefan" problem. In this problem, diffusion is only of oxygen through SiO_2. It might be modeled as an annulus, or perhaps a hollow cylinder, with the center of the problem being a boundary where all oxygen that comes into contact with it is immediately used up. In fact, oxygen coming into contact with Si is immediately converted to SiO_2, so the Si/SiO_2 interface is constantly changing, growing outward.

Another aspect of this problem is the bulk modulus of Si and SiO_2. As new SiO_2 is made beneath the previous layer, it expands to an amount larger than the original Si cylinder (SiNW), putting force on the SiO_2 layer around it. Since this takes place at a high temperature, the forces will not be as great as they would be at room temperature, and in fact, the high temperature will help the SiO_2 layer above stretch and change to accommodate the growing layer beneath. This is quite far from the traditional oxidation problem, where planar Si is oxidized and any movement

of the oxide layer is inconsequential, since there is no force resisting growth of new layers of oxide beneath the old.

We see also, from the results of Chapter 4, that the diffusion of oxygen into the cylindrical SiO_2 layers is different from that of planar Si. We know also that the oxidation rates for Boron and Phosphorus are different, as well as the oxidation rates for <100>, <110> and <111> aligned Si. While the rate of diffusion was only about 90% for planar Si as that of cylindrical Si, we also know that modifications to the diffusion process tend to intensify this difference, as observed in the drive-in formulas. There remains a good deal of work to do on this matter.

Diffusion

In Chapter 4, we discussed the diffusion of Boron and Phosphorus in SiNWs, using Fick's laws and a number of solutions, based on the initial conditions, final conditions, boundary conditions and morphology of the problems. A comparison of the two sets of diffusion formulae showed that the formulae used for planar Si cannot be used for SiNWs (cylindrical Si). What was left out of these calculations was compensation for the oxidation/drive-in process, which results in a pile-up or pile-down, as the case may go, because of the respective diffusivities of Boron and Phosphorus in SiO_2. It was easy enough to produce a solution to the drive-in problem, as long as the diffusivities of Boron and Phosphorus in SiO_2 were the same as that for Si. Etch off the oxidation layer and the answer is right there, except that it left out some key diffusion processes. While this problem was pursued aggressively in this thesis, a valid solution was not found (a solution was found, but it was rejected and left out of this thesis for its lack of strong scientific rigor).

Two significant problems turn up in pursuit of a solution to this problem. The lesser problem is that of the Phosphorus diffusion, in which the oxide layer simply pushes almost all of the Phosphorus into the Si, because of its low diffusivity. Some of the dopant is left behind, but the ratio is so small as to be small enough to call it zero (0). This will solve a minor problem. The larger part of this problem is that of determining how the diffusion of dopant caught in the oxide layer is to be affected in the Si layer. One approach (used during this investigation but not presented here) was to approximate the diffusion as taking place in a shorter period (say, instead of ten minutes, as used in this model, one-thirtieth of that, or t/30) and to do this calculation with a planar equation (a cylindrical formula was not available). Apply this calculation as a superposition with the existing diffusion profile, and then plot. This seemed to work well and even demonstrated a pile-up that was observed in other publications, but it had its problems, the main one being that of lacking a scientific basis for the secondary diffusion profile.

A similar problem occurs with Boron, except that in this case, if the numbers are added up, in the simplest sense, there is not enough Boron in the entire sample, already diffused or otherwise, to feed the ravenous hunger of the oxide layer for Boron. This suggests a complete recalculation of the originating diffusion profile (the pre-dep), perhaps even changing N_0, the surface concentration, and then do two separate formulas for diffusion. The output would again be a superposition of the two solutions. A post-oxidation profile would eliminate the oxide layer and all of the dopant contained within, which is expected to be most of it. One large concern with this approach is the lack of experimental data to support the results. There are a number of reports (mentioned in Chapter 4) on the diffusion of Boron in SiNWs, but at this point, only one of these seems to have a logical approach to this problem.

Agglomeration

The agglomeration of SiNWs is one of their main features, whether good or bad. It seems, in many cases, in order to make SiNWs useful, that it would be desirable to be able to undo the entanglements of agglomerated SiNWs. Some attempts were made, prior to this thesis, to do this, which ended with less than ideal results. It still remains a problem that needs to be dealt with, one way or another. From Chapter 2, we see that SiNWs can be made that are not agglomerated, but instead, single spires, standing in lone fields of tiny, stunted SiNWs. This is one result, but somewhere between this and the agglomerated SiNWs of the next size up, is a stand of single SiNWs, separate and individual. This is only one solution, and it may not be the best. Other solutions involve the passivation of SiNWs during the growth process. Agglomeration is said to be caused by the van der Waals forces, which have been shown to be inhibited by the use of ozone during the growth process of nano-materials – specifically, Polypyrrole nanospheres [85].

Experimental Verification

One final issue is that of experimental verification. In Chapter 4, the literature search revealed a number of methods used to measure the doping profiles of SiNWs, most of which appeared to be valid, if complex and somewhat reliable, methods of doing so. Each had a commonality, which was that of having been made by the gold-catalyzed VLS method (bottom-up). Since the SiNWs made in this thesis are made by the electroless etching (top-down) method, most of the measurement methods devised by other research groups will not work for this morphology. In the VLS method, SiNWs size (diameter) and even shape (i.e. conical) are

fairly well controllable, which allows the measurement techniques to be used. In the electroless etching method, neither size nor shape can be controlled, which renders those techniques mostly useless. In this research, some small victory has been achieved in that regard, that we have gained some small amount of control over these morphological bits.

APPENDIX A: ELSEVIER STATEMENT OF AUTHOR COPYRIGHTS

ELSEVIER

http://www.elsevier.com
About Elsevier > Authors' Rights & Responsibilities

Authors' Rights & Responsibilities

At Elsevier, we are dedicated to protecting your rights as an author, and ensuring that any and all legal information and copyright regulations are addressed.

Whether an author is published with Elsevier or any other publisher, we hold ourselves and our colleagues to the highest standards of ethics, responsibility and legal obligation.

As a journal author, you retain rights for a large range of author uses of your article, including use by your employing institute or company. These rights are retained and permitted without the need to obtain specific permission from Elsevier.

- Intellectual property
- Your role
- Permissions
- Publishing ethics
- Other policies

Copyright
Intellectual property, in particular copyright (rights in editorial content), trademarks (rights in brands for services or journals), and database rights (rights in compilations of information), form the foundation of Elsevier's publishing services and communications businesses. We in Elsevier embrace the opportunities the digital environment offers for communication and access, while at the same time we recognize the new risks that this environment poses, that being the ease with which unauthorized copies can be made and distributed worldwide. Download your practical guide to Elsevier's copyright policy.

Our objective
We aim to manage digital rights and brands amidst the structural changes that the "information society" represents, while at the same time recognizing the shared goals we have with our customers and authors. These include providing the widest possible distribution of scientific and medical content and services in a financially sustainable business model.

Elsevier wants to ensure a proper balance between the scholarly rights which authors retain (or are granted/transferred back in some cases) and the rights granted to Elsevier that are necessary to support our mix of business models. We routinely analyse and modify our policies to ensure we are responding to authors' needs and concerns, and to the concerns in general of the research and scholarly communities.

What rights do I retain as a journal author*?

- the right to make copies (print or electronic) of the journal article for your own personal use, including for your own classroom teaching use;
- the right to make copies and distribute copies of the journal article (including via e-mail) to research colleagues, for personal use by such colleagues for scholarly purposes*;
- the right to post a pre-print version of the journal article on Internet websites including electronic pre-print servers, and to retain indefinitely such version on such servers or sites for scholarly purposes* (with some exceptions such as The Lancet and Cell Press. See also our information on electronic preprints for a more detailed discussion on these points)*;
- the right to post a revised personal version of the text of the final journal article (to reflect changes made in the peer review process) on your personal or institutional website or server for scholarly purposes*, incorporating the complete citation and with a link to the Digital Object Identifier (DOI) of the article (but not in subject-oriented or

centralized repositories or institutional repositories with mandates for systematic postings unless there is a specific agreement with the publisher. ⊟→Click here for further information);

- the right to present the journal article at a meeting or conference and to distribute copies of such paper or article to the delegates attending the meeting;
- for your employer, if the journal article is a 'work for hire', made within the scope of the author's employment, the right to use all or part of the information in (any version of) the journal article for other intra-company use (e.g. training);
- patent and trademark rights and rights to any process or procedure described in the journal article;
- the right to include the journal article, in full or in part, in a thesis or dissertation;
- the right to use the journal article or any part thereof in a printed compilation of your works, such as collected writings or lecture notes (subsequent to publication of the article in the journal); and
- the right to prepare other derivative works, to extend the journal article into book-length form, or to otherwise re-use portions or excerpts in other works, with full acknowledgement of its original publication in the journal.

***Commercial purposes and systematic distribution**
Authors of Elsevier-published articles may use them only for scholarly purposes as set out above and may not use or post them for commercial purposes or under policies or other mechanisms designed to aggregate and openly disseminate manuscripts or articles or to substitute for journal-provided services. This includes the use or posting of articles for commercial gain or to substitute for the services provided directly by the journal including the posting by companies of their employee-authored works for use by customers of such companies (e.g. pharmaceutical companies and physician-prescribers); commercial exploitation such as directly associating advertising with such postings; the charging of fees for document delivery or access; the systematic distribution to others via e-mail lists or list servers (to parties other than known colleagues), whether for a fee or for free; the posting of links to sponsored articles by commercial third parties including pharmaceutical companies; institutional, funding body or government manuscript posting policies or mandates that aim to aggregate and openly distribute the accepted, peer reviewed manuscripts or published journal articles authored by its researchers or funded researchers; and subject repositories that aim to aggregate and openly distribute accepted peer reviewed manuscripts or published journal articles authored by researchers in specific subject areas.

For a more detailed discussion of our article posting policies and the different stages of a journal article development that are relevant from a policy perspective, please see the ⊟→ Article Posting Policies information page.

When Elsevier changes its journal usage policies, are those changes also retroactive?
Yes, when Elsevier changes its policies to enable greater academic use of journal materials (such as the changes several years ago in our web-posting policies) or to clarify the rights retained by journal authors, Elsevier is prepared to extend those rights retroactively with respect to articles published in journal issues produced prior to the policy change.

We are pleased to confirm that, unless explicitly noted to the contrary, all policies apply retrospectively to previously published journal content. If, after reviewing the material noted above, you have any questions about such rights, please contact Global Rights.

How do I obtain a Journal Publishing Agreement?
You will receive a form automatically by post or e-mail once your article is received by Elsevier's Editorial-Production Department. View a generic example of the agreement. Some journals will use another variation of this form.

Why does Elsevier request transfer of copyright?
The research community needs certainty with respect to the validity of scientific papers, which is normally obtained through the editing and peer review processes. The scientific record must be clear and unambiguous. Elsevier believes that, by obtaining copyright transfer, it will always be clear to researchers that when they access an Elsevier site to review a paper, they are reading a final version of the paper which has been edited, peer-reviewed and accepted for publication in an appropriate journal. This eliminates any

ambiguity or uncertainty about Elsevier's ability to distribute, sub-license and protect the article from unauthorized copying, unauthorized distribution, and plagiarism.

Can you provide me with a PDF file of my article?
Many Elsevier journals are now offering authors e-offprints – free electronic versions of published articles. E-offprints are watermarked PDF versions, and are usually delivered within 24 hours, much quicker than print copies. These PDFs may not be posted to public websites. For more information, please see your journal's Guide to Authors or contact sciencereprints@elsevier.com

APPENDIX B: ECS COPYRIGHT PERMISSION

Request for Permission to Reproduce or Re-Publish ECS Material

I am preparing a **dissertation** entitled: ***Characterization, Morphology, Oxidation and Recession of Silicon Nanowires Grown by Electroless Process,***
to be published by: **University of Central Florida, Orlando, FL**
in an upcoming publication entitled; Electronic Thesis and Dissertation (ETD).

I request permission to use the following material in the publication noted above, and request non-exclusive rights for all subsequent editions and in all foreign language translations for distribution throughout the world.

Description of material to be used: In whole or in part, all text, figures, tables, formulas in a single chapter (Abstract and References may be moved to a separate section of the dissertation) as part of a doctoral dissertation, this yet-to-be-published work by R.G. Mertens, K. B. Sundaram, R. G. Blair, ***Recession and Characterization of Patterned Nanowires by Electroless Etching of Silicon***, ECS Journal of Solid State Science and Technology (JSS), Vol. **1**, Issue (1), (unknown pages) (2012), accepted for Publication (JSS-12-0109).

Signature: _____ Date: 5/29/12

Name: Robert G. Mertens
Address: 1400 Hartley Ave., Deltona, FL 32725
Home: 386-860-0345
Email: quarkmaster@gmail.com
bubmertens@knights.ucf.edu

Permission is granted to reproduce the above-referenced material. Please acknowledge the author(s) and publication data of the original material, and include the words: "Reproduced by permission of The Electrochemical Society."

June 1, 2012
Date

Ann F. Goedkoop
Ann F. Goedkoop, Director of Publications

APPENDIX C: MATHEMATICAL FUNCTIONS

Bessel Functions

A graph of the zeroth order Bessel function of the first kind [86] is shown in Figure 16 and is described by

$$J_0(x) = \sum_{m=0}^{\infty} \frac{(-1)^m (x/2)^{2m}}{m!\Gamma(m+1)} \tag{C.1}$$

A graph of the first order Bessel function of the first kind [86] is shown in Figure 17 and id described by

$$J_1(x) = \sum_{m=0}^{\infty} \frac{(-1)^m (x/2)^{2m+1}}{m!\Gamma(m+2)} \tag{C.2}$$

In order for Bessel functions to be useful, their zeros must be known. Bessel zeros for zeroth and first order Bessel functions to the first kind is shown in Table 5.

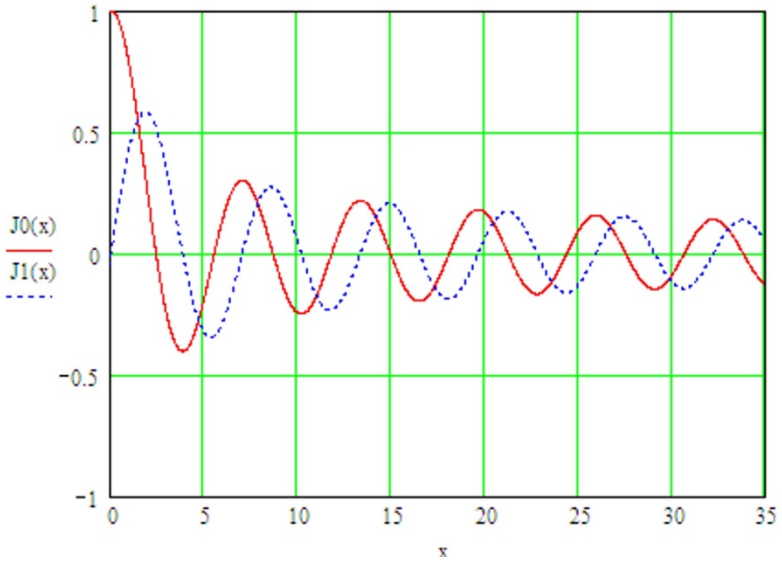

Figure 23 Graph of the zeroth, $J_0(x)$, and first, $J_1(x)$, order Bessel functions of the first kind.

Table 5 First 11 zeros of zeroth and first order Bessel functions of the first kind

k	$J_0(x)$	$J_1(x)$
1	2.4048	0
2	5.5201	3.8317
3	8.6537	7.0156
4	11.7915	10.1735
5	14.9309	13.3237
6	18.0711	16.4706
7	21.2116	19.6159
8	24.374	22.76
9	27.467	25.909
10	30.664	29.049
11	33.774	32.195

Error Functions

A graph of the error function [86] is shown in Figure 17 and is described by

$$\mathrm{erf}(x) = \frac{2}{\sqrt{\pi}} \int_0^x e^{-t^2} dt \qquad -\infty < x < \infty \tag{C.3}$$

A graph of the complimentary error function [86] is shown in Figure 18 and is described by

$$\mathrm{erfc}(x) = \frac{2}{\sqrt{\pi}} \int_x^\infty e^{-t^2} dt \qquad -\infty < x < \infty \tag{C.4}$$

The Gamma Function

The gamma function [86] is used in the zeroeth and first order Bessel functions of the first kind, shown above. A graph of the gamma function is shown in Figure 19 and is described by

$$\Gamma(x) = \int_0^x e^{-t} t^{x-1} dt \tag{C.5}$$

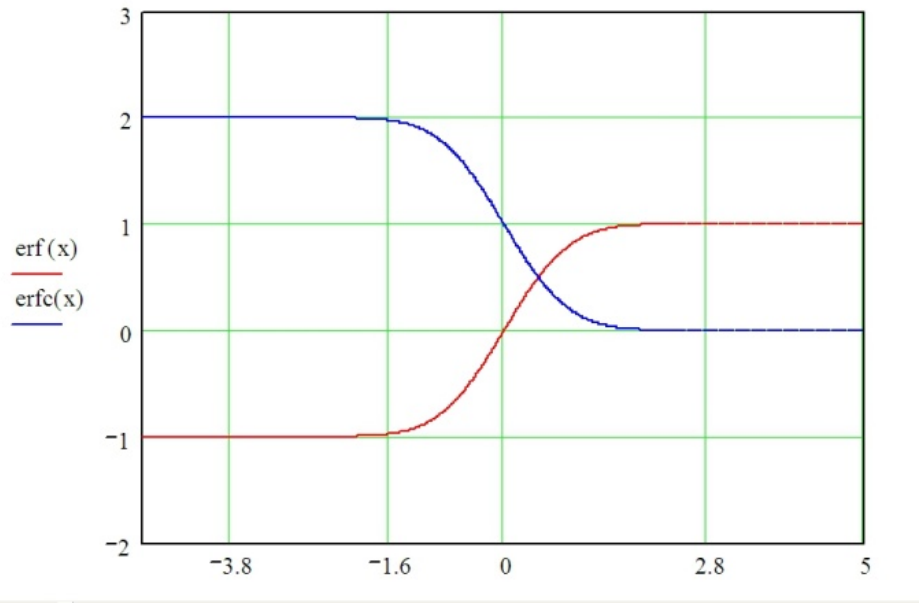

Figure 24 Graphs of the error function, erf(x), and the complimentary error function erfc(x).

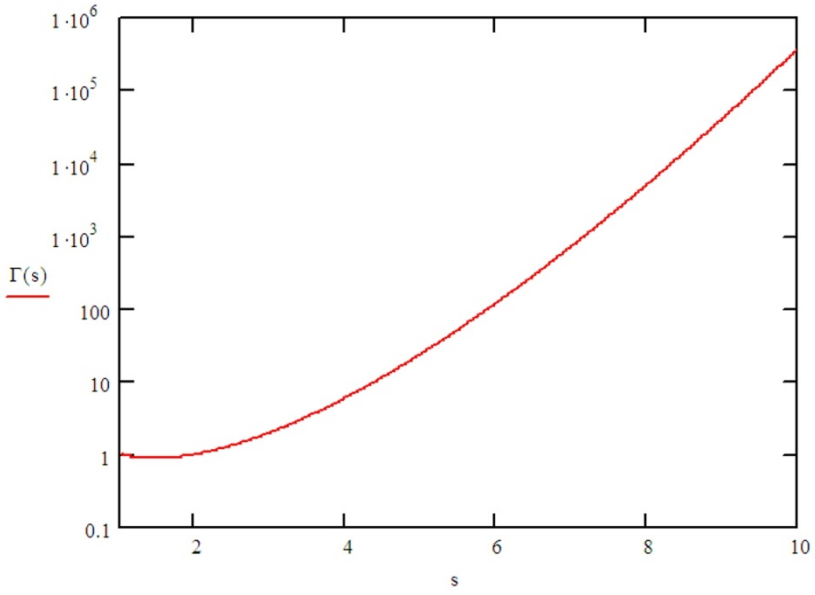

Figure 25. Graph of the gamma function, Γ(x).

Fourier Series

A converging Fourier series [86] is used to construct a periodic function known as a square wave, although by the strictest definition, this is not a square wave, but rather an approximation to one. The converging Fourier series is shown in the graph of Figure 20 and is described by the function

$$S_N(x) = \frac{1}{2} + \frac{2}{\pi}\sum_{n=1}^{N}\frac{\sin[(2n-1)\pi)]}{(2n-1)} \qquad \text{(C.6)}$$

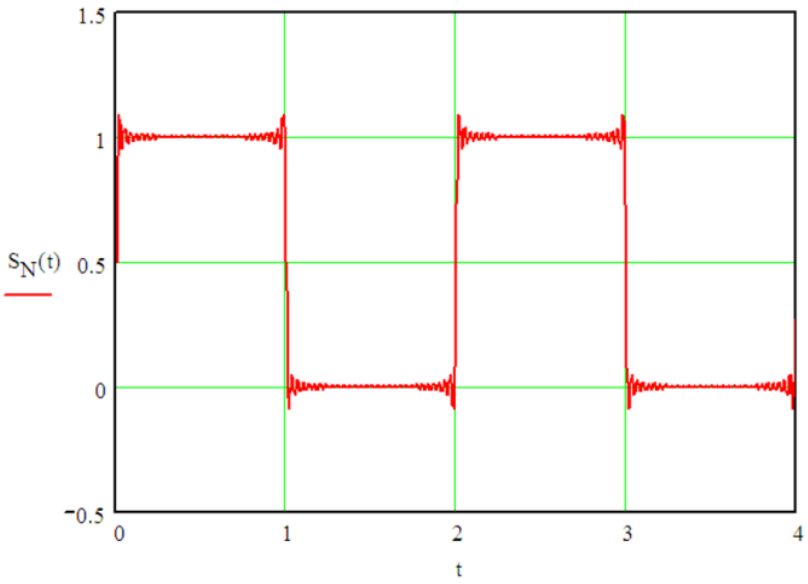

Figure 26. Graph of a converging Fourier series function.

The Heaviside Function

The Heaviside function is used to create a step and is more easily recognized by its common title, the *step function.* A graph of the Heaviside function is shown in Figure 21 and is described by

$$\Phi(x) = \begin{cases} 0, x < 0 \\ 1/2, x = 0 \\ 1, x > 0 \end{cases} \tag{C.7}$$

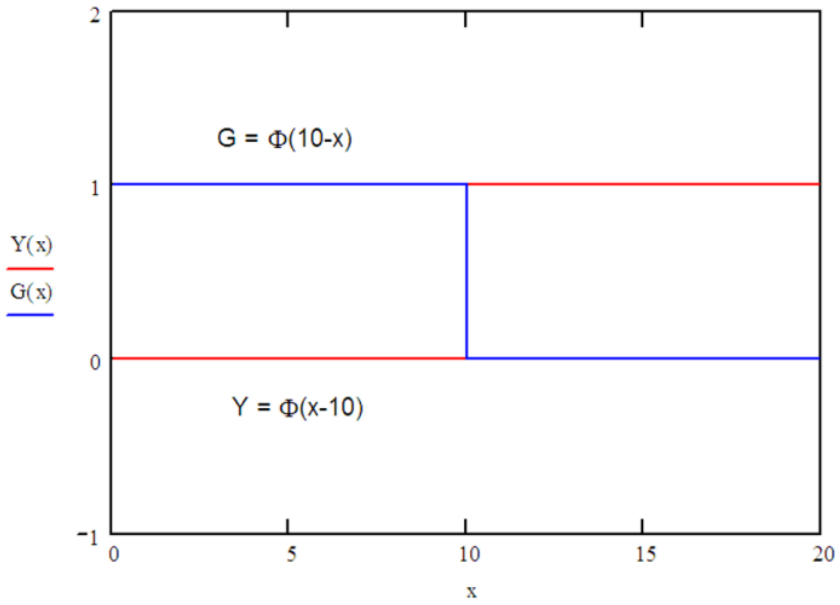

Figure 27. The Heaviside function is also called a *step function.*

GENERAL REFERENCES

R. A. Serway, *Physics for Scientists and Engineers*, 2nd Ed. Saunders College Publishing, New York, 1982.

F. Bowman, *Introduction to Bessel Functions*, Dover Publications, Inc. New York, 1958.

REFERENCES

[1] L. T. Canham, *Silicon quantum wire array fabrication by electrochemical and chemical dissolution of wafers*, Appl. Phys. Lett. **57**, 1046 (1990).

[2] K. Q. Peng, Y-J. Yan, S-P. Gao and J. Zhu, *Synthesis of Large-Area Silicon Nanowire Arrays via Self-Assembling Nanoelectrochemistry*, Adv. Mater. (Weinheim, Ger.)., **14** (16) 1164 (2002).

[3] A. I. Hochbaum, R. Chen, R. D. Delgado, W. Liang, E. C. Garnett, M. Najarian, A. Majumdar and P. Yang, *Enhanced thermoelectric performance of rough silicon nanowires*, Nature, **451**, pp. 163-167 (2008).

[4] X. L., Beng K. Tay, G. You and Y. Yang, *A simple method to fabricate silicon nanowire arrays by a catalytic electrochemical etching process*, 2nd IEEE International Nanoelectronics Conference (INEC 2008), (2008).

[5] K. Peng, M. Zhang, A. Lu, N-B. Wong, R. Zhang and S-T. Lee, *Ordered silicon nanowire arrays via nanosphere lithography and metal-induced etching*, Appl. Phys. Lett., **90**, 163123 (2007).

[6] H. Schmid, M. T. Björk, J. Knoch, H. Riel, W. Riess, P. Rice and T. Topuria, *Patterned epitaxial vapor-liquid-solid growth of silicon nanowires on Si(111) using silane*, J. Appl. Phys., **103**, 024304 (2008).

[7] T. Mårtensson, P. Carlberg, M. Borgstrolm, L. Montelius, W. Seifert, and L. Samuelson, *Nanowire Arrays Defined by Nanoimprint Lithography*, Nano Lett. **4**, 699 (2004).

[8] N. Wang, Y. Cai and R. Q. Zhang, *Growth of Nanowires*, Mater. Sci. Eng., R **60**, 1 (2008).

[9] D. Kumar, S. K. Srivastava, P. K. Singh, M. Husain and V. Kumar, *Fabrication of silicon nanowire arrays based solar cell with improved performance*, Sol. Energy Mater. Sol. Cells, **95,** 215 (2011).

[10] V. A. Sivikov, F. Voigt, A. Berger, G. Bauer and S. H. Christiansen, *Roughness of silicon nanowire sidewalls and room temperature photoluminescence*, Phys. Rev. B, **82** 125446 (2010).

[11] Y. Chao, *1.16 Optical Properties of Nanostructured Silicon*. In: D. L. Andrews, G. D. Scholes and G. P. Wiederrecht (eds.), *Comprehensive Nanoscience and Technology, Volume 1*., pp. 543-570 Oxford: Academic Press, (2011).

[12] B. E. Deal & A. S. Grove, *General Relationship for the Thermal Oxidation of Silicon*, J. App. Phy. **36**, No. 12 (1965).

[13] H. Z. Massoud, J. D. Plummer and E. A. Irene, *Thermal Oxidation of Silicon in Dry Oxygen Growth Rate Enhancement in the Thin Regime*, J. Electrochem. Soc., Nov. pp. 2685-2693 (1985).

[14] H. Z. Massoud, *Growth Kinetics and Electrical Properties of Ultrathin Silicon-Dioxide Layers*, ECS Transactions, **2** (2), pp. 189-203 (2006).

[15] H. Z. Massoud and J. D. Plummer, *Analytical relationship for the oxidation of silicon in dry oxygen in the thin-film regime*, J. Appl. Phys. **62** (8), Oct., pp. 3416-3423 (1987).

[16] T. Ohmi, M. Morita, A. Teramoto, K. Makihara and K.S. Tseng, *Very thin oxide film on a silicon surface by ultraclean oxidation,* Appl. Phys. Lett. **60** pp. 2126 - 2128 (1992).

[17] Y. Shi, J. L. Liu, F. Wang, Y. Lu, R. Zhang, S. L. Gu, P. Han, L. Q. Hu, Y. D. Zheng, C. Y. Lin and D. A. Du, *Ultrafine silicon quantum wires fabricated by selective chemical etching and thermal oxidation*, J. Vac. Sci. Technol. A **14**(3), May/Jun, pp. 1194-1198 (1996).

[18] K. Kim, Y. H. Lee, M. H. An, M. S. Suh, C. J. Youn, K. B. Lee and H. J. Lee, *Growth law of silicon oxides by dry oxidation*, Semicond. Sci. Technol. **11** pp. 1059–1064 (1996).

[19] H. Z. Massoud, J. D. Plummer and E. A. Irene, *Thermal Oxidation of Silicon in Dry Oxygen*, J. Electrochem. Soc., **132** No. 7, pp. 1745-1753 (1985).

[20] E. A. Lewis and E. A. Irene, *The Effect of Surface Orientation on Silicon Oxidation Kinetics*, J. Electrochem. Soc., Solid State Sci. and Tech., **134** No. 9, pp. 2332-2339 (1987).

[21] R. C. Jaeger, *Volume V: Introduction to Microelectronic Fabrication, 2nd. Ed. Modular Series on Solid State Devices*, Prentice Hall, Upper Saddle River, New Jersey 07458

[22] M. D. McCluskey, E. E. Haller, *Dopants and Defects in Semiconductors*, CRC Press, Taylor & Francis Group, Boca Raton, Florida (2012).

[23] A. Fick, *Ueber Diffusion (In German)*, Annalen Der Physik, **170** 1 pp 59-86, (1855).

[24] A. Fick, *On Liquid Diffusion (In English)*, Phil. Mag. **10** 30 (1855).

[25] H. Mehrer, *Diffusion in Solids; Fundamentals, Methods, Materials, Diffusion-Controlled Processes*, Springer-Verlag Berlin Heidelberg (2007).

[26] H. S. Carslaw, J. C. Jaeger, *Conduction of Heat in Solids, 2nd. Ed.*, Oxford at Clarendon Press, Oxford University Press, Amen House, London E.C.4 (1959).

[27] J. Crank, *The Mathematics of Diffusion*, Oxford University Press, Amen House, London, E.C. 4, (1956).

[28] P. G. Shewmon, *Diffusion in Solids*, McGraw-Hill Book Company, New York (1963).

[29] R. J. Borg, G. J. Dienes, *An Introduction to Solid State Diffusion*, Academic Press, Inc., San Diego (1988).

[30] G. E. Murch, *Diffusion in Solids: Unsolved Problems*, Trans Tech Publications, Ltd., Zurich (1992).

[31] A. Õchsner and J. Grácio (eds.), *Diffusion in Solids and Liquids, Heat Transfer – Microstructure & Properties*, Trans Tech Publications, Zurich (2007).

[32] J. E. Shelby, *Handbook of Gas Diffusion in Solids and Melts*, ASM International, Materials Park, Ohio (1996).

[33] J. Crank, *Free and Moving Boundary Problems*, Clarendon Press, Oxford, 1984.

[34] H. P. W. Gottlieb, *Exact Solution of a Stefan Problem in a Nonhomogeneous Cylinder*, Appl. Math. Lett., Vol 15, 2, pp. 167-172 (2002).

[35] S. C. Gupta, *The Classical Stefan Problem: Basic Concepts, modelling and analysis*, Elsevier Science BV (2003).

[36] E. Koren, N. Berkovitch and Y. Rosenwaks, *Measurement of Active Dopant Distribution and Diffusion in Individual Silicon Nanowires*, Nano Lett. **10** 4 p. 1163 (2010).

[37] D. E. Perea, E. R. Hemesath, E. J. Schwalbach, J. L. Lensch-Falk, P. W. Voorhees and L. J. Lauhon, *Direct measurement of dopant distribution in an individual vapour-liquid-solid nanowire*, Nature Nanotechnology Letters, **4** (2009).

[38] J. E. Allen, D. E. Perea, E. R. Hemesath and L. J. Lauhon, *Nonuniform Nanowire Doping Profiles Revealed by Quantitative Scanning Photocurrent Microscopy*, Adv. Mater. **21** p. 3067 (2009).

[39] G. Imamura, T. Kawashima, M. Fujii, C. Nishimura, T. Saitoh and S. Hayashi, *Distribution of Active Impurities in Single Silicon Nanowires*, Nano Lett. **8** (9) p. 2620 (2008).

[40] E. C. Garnett, Y-C. Tseng, D. R. Khanal, J. Wu, J. Bokor and P. Yang, *Dopant profiling and surface analysis of silicon nanowires using capacitance-coltage measurements*, Nature Nanotechnology Letters, **4** p. 311 (2009).

[41] R. G. Mertens, K. B. Sundaram, *Recession and Characterization of Nanowires Grown by Electroless Etching of Silicon*, Meet. Abstr. – Electrochem. Soc. **1101** 123 (2011).

[42] R. G. Mertens, K. B. Sundaram, *Recession and Characterization of Patterned Nanowires Grown by Electroless Etching of Silicon*, ECS Trans. **35** (10), 63 (2011).

[43] R. G. Mertens, K. B. Sundaram, R. G. Blair, *Recession and Characterization of Patterned Nanowires Grown by Electroless Etching of Silicon*, Accepted for publication in ECS Journal of Solid State Science and Technology (JSS), **1** (1) (page no. not available, first publication of JSS on July 17th) (2012).

[44] Y. Wu and P. Yang, *Direct Observation of Vapor-Liquid-Solid Nanowire Growth*, J. Am. Chem. Soc.**, 123**, pp. 3165-3166 (2001).

[45] M. K. Sunkara, S. Sharma, R. Miranda, G. Lian, and E. C. Dickey, *Bulk synthesis of Silicon Nanowires using a low-temperature vapor-liquid-solid method*, Appl. Phys. Lett. **79**, 1546 (2001).

[46] Y. Wang, V. Schmidt, S. Senz, and U. Gösele, *Epitaxial growth of silicon nanowires using an aluminum catalyst*, Nat. Nanotechnol. **1,** pp. 186-189 (2006).

[47] J. B. Hannon, S. Kodambaka, F. M. Ross and R. M. Tromp, *The influence of the surface migration of gold on the growth of silicon nanowires*, Nature **440**, pp. 69-71 (2006).

[48] F. Iacopi, P. M. Vereecken, M. Schaekers, M. Caymax, N. Moelans, B. Blanpain, O. Richard, C. Detavernier and H. Griffiths, *Plasma-enhanced chemical vapor deposition growth of Si nanowires with low melting point metal catalysts: an effective alternative to Au-mediated growth*, Nanotechnology **18,** 505307 (2007).

[49] I. Zardo, L. Yu, S. Conesa-Boj, S. Estradé, P. J. Alet, J. Rössler, M. Frimmer, P. R. i Cabarrocas, F. Peiró, J. Arbiol, J. R. Morante and A. F. i Morral, *Gallium assisted plasma*

enhanced chemical vapor deposition of silicon nanowires, Nanotechnology **20**, 155602 (2009).

[50] K. Q. Peng, Y. J. Yan S. P. Gao and J. Zhu, *Dendrite-Assisted Growth of Silicon Nanowires in Electroless Metal Deposition*, Adv. Funct. Mater.**13**, (2) pp. 127-132 (2003).

[51] K. Peng and J. Zhu, *Simultaneous gold deposition and formation of silicon nanowire arrays*, J. Electroanal. Chem.. **558,** pp. 35-39 (2003).

[52] K. Peng, H. Fang, J. Hu, Y. Wu, J. Zhu, Y. Yan, and S. T. Lee, *Metal-Particle-Induced, Highly Localized Site-Specific Etching of Si and Formation of Single-Crystalline Si Nanowires in Aqueous Fluoride Solution*, Chem.--Eur. J.. **12**, (30) pp. 7942-7947 (2006).

[53] T. Qiu, X.L. Wu, Y. F. Mei, G. J. Wan, P. K. Chu and G. G. Siu, *From Si nanotubes to nanowires: Synthesis, characterization and self-assembly*, J. Cryst. Growth **277,** pp. 143-148 (2005).

[54] E. A. Dalchiele, F. Martín, D. Leinen, R. E. Marotti, and J. R. Ramos-Barradob, *Single-Crystalline Silicon Nanowire Array-Based Photoelectrochemical Cells*, J. Electrochem. Soc.., **156** K77 (2009).

[55] K. Peng, X. Wang, and S-T Lee, *Silicon nanowire array photoelectrochemical solar cells*, Appl. Phys. Lett .**92**, 163103 (2008).

[56] American Society for Testing and Materials (ASTM) *ASTM G173*, (2008).

[57] L. Tsakalakos, J. Balch, J. Fronheiser, B. A. Korevaar, O. Sulima and J. Rand, *Silicon nanowire solar cells*, Appl. Phys. Lett., **91**, 233117 (2007).

[58] M. Nolan, S. O'Callaghan, G. Fagas, and J. C. Greer, *Silicon Nanowire Band Gap Modification*, Nano Lett. **7** (1) pp. 34-38 (2007).

[59] Z. Gao, A. Agarwal, A. D. Trigg, N. Singh, C. Fang, C-H Tung, Y. Fan, K. D. Buddharaju, and J. Kong, *Silicon Nanowire Arrays for Label-Free Detection of DNA*, Anal. Chem., **79** (9) pp. 3291-3297 (2007).

[60] M. N. Masood, S. Chen, E. T. Carlen, and A. van den Berg, *All-(111) Surface Silicon Nanowires: Selective Functionalization for Biosensing Applications*, ACS Appl. Mater. Interfaces, **2**, (12) pp. 3422-3428 (2010)

[61] J. Li, Y. Zhang, S. To, L. You, and Y. Sun, *Effect of Nanowire Number, Diameter and Doping Density on Nano-FET Biosensor Sensitivity,* ACS Nano, **5** (8) pp. 6661-6668 (2011).

[62] S. Singh, J. Zack, D. Kumar, S. K. Srivastava, Govind, D. Saluja, M. A. Khan and P. K. Singh, *DNA hybridization on silicon nanowires*, Thin Solid Films **519** (3) pp. 1151-1155 (2010).

[63] H. Fang, Y. Wu, J. Zhao and J. Zhu, *Silver catalysis in the fabrication of silicon nanowire arrays*, Nanotechnology **17** (14) pp. 3768-3774 (2006).

[64] C. Benoit-Moez, S. Bastide, and C. Levy-Clement, *Formation of Si Nanowire Arrays by Metal-Assisted Chemical Etching*, ECS Trans. **16** (3) pp. 245-252 (2008).

[65] D. Kumar, S. Srivastava, P. Singh, K. Sood, V. Singh, N. Dilawar, and M. Husain, *Room temperature growth of wafer-scale silicon nanowire arrays and Raman charactersitics,* J. Nanopart. Res. **12** (6) pp. 2267-2276 (2010).

[66] R. G. Mertens, K. B. Sundaram, *Mathematical characterization of oxidized crystalline silicon nanowires grown by electroless process,* Appl. Surf. Sci., **258**, (10) pp. 46074613 (2012).

[67] S-C. Shiu, C-Y. Hsiao, C-H. Chao, S-C. Hung, C-F. Lin, *Nanoscale Photonic and Cell Technologies for Photovoltaics*, Proceedings of SPIE **7047**, 70470F-1 (2008).

[68] J. L. Silverberg, *A model for conductive percolation in ordered nanowire arrays*, J. Appl. Phys. **105** (4) 044306 (2009).

[69] General Electric Co., *Residential Brilliance Brochure*, Brochure # GEA-17026 (07/08).

[70] Y. Zheng, C. Rivas, R. Lake, K. Alam, T. B. Boykin and G. Klimeck, *Electronic Properties of Silicon Nanowires*, IEEE Trans On Electron Dev., **52**, No. 6, (2005).

[71] T-W. Kim, C-H. Cho, B-H. Kim, and S-J. Park, *Quantum confinement effect in crystalline silicon quantum dots in silicon nitride grown using SiH_4 and NH_3*, Appl. Phy. Lett. **88**, 123102 (2006).

[72] S. Y. Ren, *Electronic States in Crystals of Finite Size: Quantum Confinement of Bloch Waves*, Springer Tracts in Modern Physics, **212**, Springer Science + Business Media, (2006).

[73] T. Takagahara and K. Takeda, *Theory of the quantum confinement effect on excitons in quantum dots of indirect-gap materials*, Phys. Rev. B 46, 15578 - 15581 (1992).

[74] T-Y. Kim, N-M. Park, K-H. Kim, G. Y. Sung, Y-W. Ok, T-Y. Seong and C-J. Choi, *Quantum confinement effect of silicon nanocrystals in situ grown in silicon nitride films*, App. Phys. Lett., **85**, No. 22, (2004).

[75] T. van Buuren, L. N. Dinh, L. L. Chase, W. J. Siekhaus, and L. J. Terminello, *Changes in the Electronic Properties of Si Nanocrystals as a Function of Particle Size*, Phy. Rev. Lett., **80**, No. 17, (1998).

[76] V. Lehmann and U. Gijsele, *Porous silicon formation: A quantum wire effect*, Appl. Phys. Lett. **58** (8), (1991).

[77] V. A. Sivakov, G. Bronstrup, B. Pecz, A. Berger, G. Z. Radnoczi, M. Krause,| and S. H. Christiansen, *Realization of Vertical and Zigzag Single Crystalline Silicon Nanowire Architectures*, J. Phys. Chem. C 3798, 114, 3798–3803 (2010).

[78] C. C. Büttner and M. Zacharias, *Retarded oxidation of Si nanowires*, Appl. Phys. Lett. **89**, 263106, (2006).

[79] J. Westwater, D. P. Gosain, S. Tomiya, S. Usui and H. Ruda, *Growth of silicon nanowires via gold/silane vapor–liquid–solid reaction*, J. Vac.Sci. Technol. B, **15**, 554 (1997).

[80] N. M. Hwang, W.S. Cheongc, D.Y. Yoonc and D-Y Kima, *Growth of silicon nanowires by chemical vapor deposition: approach by charged cluster model*, J. Cryst. Growth, **218**, Iss. 1, (2000).

[81] B. Liu, Y. Wang, T-T. Ho, K-K. Lew, S. M. Eichfeld, J. M. Redwing, T. S. Mayer and S. E. Mohney, *Oxidation of silicon nanowires for top-gated field effect transistors*, J. Vac. Sci. Technol. A **26,** 3 (2008).

[82] D. Shir, B. Z. Liu, A. M. Mohammad, K. K. Lew and S. E. Mohney, *Oxidation of silicon nanowires*, J. Vac. Sci. Technol. B **24,** (3), (2006).

[83] H. I. Liu, D. K. Biegelsen, N. M. Johnson, F. A. Ponce and R. F. W. Pease, *Self-limiting oxidation of Si nanowires*, J. Vac. Sci. Technol. B, **11**(6), pp. 2532-2537 Nov/Dec (1993).

[84] K. Sakamoto, K. Nishi, F. Ichikawa, and S Ushio, *Segregation and transport coefficients of impurities at the Si/SiO_2 interface*, J. Appl. Phys. **61** (4) (1987).

[85] C. A. Vetter, A. Suryawanshi, J. R. Lamb, B. Law, and V. J. Gelling, *Novel Synthesis of Stable Polypyrrole Nanospheres Using Ozone*, *Langmuir*, **27** (22) p. 13719 (2011).

[86] L. C. Andrews, R. L. Phillips, *Mathematical Techniques for Engineers and Scientists*, SPIE Press, Bellingham, Washington, USA, (2003).